

# Fundamental Limits of Deep Learning-Based Binary Classifiers Trained with Hinge Loss

Tilahun M. Getu, *Member, IEEE*, Georges Kaddoum, *Senior Member, IEEE*,  
and Mehdi Bennis, *Fellow, IEEE*

**Abstract**—Although deep learning (DL) has led to several breakthroughs in many disciplines, the fundamental understanding on why and how DL is empirically successful remains elusive. To attack this fundamental problem and unravel the mysteries behind DL's empirical successes, significant innovations toward a unified theory of DL have been made. Although these innovations encompass nearly fundamental advances in optimization, generalization, and approximation, no work has quantified the testing performance of a DL-based algorithm employed to solve a pattern classification problem. To overcome this fundamental challenge in part, this paper exposes the fundamental testing performance limits of DL-based binary classifiers trained with hinge loss. For binary classifiers that are based on deep rectified linear unit (ReLU) feedforward neural networks (FNNs) and deep FNNs with ReLU and Tanh activation, we derive their respective novel asymptotic testing performance limits, which are validated by extensive computer experiments.

**Index Terms**—DL, the (unified) theory of DL, interpretable AI/ML, interpretable DL, fundamental limits.

## 1 INTRODUCTION

### 1.1 Related Works

Being the most popular technology behind artificial intelligence (AI) / machine learning (ML), deep learning (DL) [1] has led to numerous 21st-century breakthroughs in many disciplines. Among those disciplines, chemistry [2], [3]; computer science [4], [5], [6]; electrical engineering [7], [8], [9]; mathematics [10], [11]; medicine [12], [13]; neuroscience [14], [15]; and physics [16], [17], [18] have witnessed DL-based breakthroughs. Despite many breakthroughs, the fundamental understanding on *why and how* DL is empirically successful in astronomically many AI/ML problems remains elusive. Nevertheless, it is widely believed that DL's empirical successes are attributable to its ability to learn salient hidden representations from the training data [19], which goes through networked layers of interconnected *closed-box processing* [20] at the heart of DL's remarkable successes in solving both classification and regression AI/ML problems. The mysteries of this black box processing are also the mysteries behind DL's empirical achievements. To uncover these mysteries, the broader multidisciplinary AI/ML research communities have made significant theoretical advancements – toward interpretable (or explainable) AI/ML – that constitute *the theory of DL* [21], [22], [23], which is concerned with *generalization, optimization, and approximation (representation) in DL* [21].

Inspired by the classical works [24], [25] that have established that feedforward neural networks (FNNs) with one hidden layer are *universal approximators*, approximation

problems, in the theory of DL, deal with deriving the approximation error bounds of one or more function approximation(s) using deep networks. In this vein, a number of recent works have established that deep FNNs – as opposed to shallow FNNs – have the power of *exponential expressivity* [26], [27], [28], [29], [30], [31]. In light of exponential expressivity, the state-of-the-art literature includes many works on deep approximation such as the width efficiency of *rectified linear unit* (ReLU) FNNs [32]; the quasi-equivalence of depth and width [33]; the universal approximation capability of slim (and sparse) networks [34]; the approximation of univariate functions by deep ReLU FNNs [35]; approximation (and estimation) using high-dimensional DL networks [36]; matrix-vector product approximation using deep ReLU FNNs [37]; universal function approximation by deep ReLU FNNs [38]; deep FNN approximation theory [39], [40]; and optimal approximation of piece-wise smooth functions using deep ReLU FNNs [41].

Apart from the aforementioned works on approximation in the context of the theory of DL, there also exist informative works (e.g., [42], [43]) on optimization in the context of the theory of DL. The authors of [44] highlight these works starting with useful developments for shallow FNNs and corroborate that there exist optimization landscape regions for discrete FNNs with only one or two layers that are both robust and accessible, and their existence is central to good training/testing performance. In addition, the authors of [45] derive various basic geometric and algorithmic features for nonconvex one- and two-layer FNNs that learn random patterns. These crucial advancements apply to shallow networks rather than the state-of-the-art practical deep networks that are often over-parameterized [43]. Even though over-parameterized deep (and shallow) networks must be *overfitted* per the classical bias-variance tradeoff [46], [47], over-fitting does not often happen with practical

T. M. Getu is with the Electrical Engineering Department, École de Technologie Supérieure (ETS), Montréal, QC H3C 1K3, Canada (e-mail: tilahun-melkamu.getu.1@ens.etsmtl.ca).

G. Kaddoum is with the Electrical Engineering Department, École de Technologie Supérieure (ETS), Montréal, QC H3C 1K3, Canada (e-mail: georges.kaddoum@etsmtl.ca).

M. Bennis is with the Centre for Wireless Communications, University of Oulu, 90570 Oulu, Finland (e-mail: mehdi.bennis@oulu.fi).

deep networks [43]. This *discrepancy*<sup>1</sup> remains as one of the fundamental issues in the theory of DL [43]. Meanwhile, several theoretical works have been published on over-parameterized deep (and shallow) networks: Convergence theory for deep ReLU FNNs [50], [51]; convergence theory for an over-parameterized ResNet [52]; the optimization landscape of over-parameterized shallow FNNs [53]; and how much over-parameterization is sufficient to learn deep ReLU FNNs [54]. Moreover, the recent theoretical works [55], [56] affirm that over-parameterization improves generalization. In harmony with this theory, the authors of [57] empirically corroborate that over-parameterized DL models can fit the training data and generalize well even when the labels are substituted by noise. Meanwhile, when it comes to generalization via implicit regularization and tractability via over-parametrization, the authors of [23] provide a statistical viewpoint.

As for generalization, state-of-the-art AI/ML research incorporates interesting works that exploit local Rademacher complexities, algorithmic stability, compression bounds, and algorithmic robustness to derive the generalization error bounds of deep (also shallow) networks [23]. The authors of [46], on the other hand, expose the existence of *double descent* that amalgamates the classical U-shaped test risk curve and the modern interpolating regime (with zero training error) for over-parameterized DL models. The authors of [58] took inspiration from double descent and revealed *triple descent*, which also comprises a superabundant parameterization regime corresponding to a deterministic NTK [48]. NTK is the limiting kernel of wide FNNs as their width approaches infinity [48]. When it comes to infinitely wide FNNs, crucial *mean field limits* are derived for two-layer FNNs [59] and multi-layer FNNs [60]. Meanwhile, the fundamental phenomena of *neural collapse* and *minority collapse* are unveiled in [61] and [62], respectively. Neural collapse is a fundamentally pervasive inductive bias that occurs during the terminal phase of training beginning at the epoch in which the training error first vanishes while the training loss is driven to zero [61], whereas minority collapse is the fundamental limit on the minority classes of DL models that are trained for an adequately long time on class-imbalanced datasets [62].

## 1.2 Motivation and Context

Foundational themes on the achievements of DL focus on the following questions: *i)* How can training forward-propagating data through deep networks impact the optimization landscape to such an extent that viable solutions (such as *good local minima*) are attained? *ii)* If a viable solution is attained w.r.t. the training data, how can we

1. Over-parameterized deep networks need to move only a tiny distance, and linearization can be a good approximation (also concerning the *neural tangent kernel* (NTK) [48]). Nonetheless, because deep networks are not ultra-wide in practice, their parameters will move a large distance that is more than the linearization regimes permit [43]. On the other hand, the authors of [49] reveal an implicit bias phenomenon dubbed *lazy training* that applies when a non-linear parametric model behaves like a linear one. This can occur implicitly under some choices of hyper-parameters governing normalization, initialization, and the number of iterations when the model is large [49].

generalize it well for unseen testing data? *iii)* When it comes to learning using the *back-propagation algorithm* [63] to solve both classification and regression AI/ML problems, how does a network trainer's choice of DL architecture, initializer, optimizer, normalization scheme, and regularization scheme interact with the training dataset(s) to influence the optimization landscape and the generalizability of a trained DL model? These questions must be carefully addressed so as to reveal the fundamental testing performance limits of a DL-based AI/ML algorithm. Therefore, quantifying the fundamental testing performance limits of a deep FNN-based AI/ML algorithm entails the quantification of the attainable optimization landscape during training and the subsequent generalization error bound.

There could be infinitely many local minima [64] for an FNN architecture and a loss function, some of which can lead to efficient learning. However, we lack a fundamental insight on which minima the optimization algorithm selects due to a lack of: *i)* understanding of training dynamics, and *ii)* mathematical tools to describe the landscape of the loss function of large FNNs [65]. Apart from these formidable challenges, the back-propagating gradients that are involved in error back-propagation are often random gradients with unknown distributions. These render the development of almost all *high-dimensional statistics* [66] nearly useless, especially when one is trying to determine the non-asymptotic testing performance limits of an FNN-based classification AI/ML algorithm.<sup>2</sup> These fundamental testing performance limits may pave the way to the rigorous interpretation of trained deep networks solving classification AI/ML problems. To the best of our knowledge, nonetheless, no fundamental works that quantify the testing performance limits of DL-based classifiers – trained with *cross-entropy loss* or *hinge loss* – have been managed yet. This is the motivation and context behind our work on the fundamental testing performance limits of FNN-based binary classifiers trained with hinge loss.

## 1.3 Contributions

This paper investigates two kinds of DL-based binary classifiers: *i)* The ones based on a deep ReLU FNN, and *ii)* the ones based on a deep FNN with a ReLU activation function in all layers except the output layer equipped with a hyperbolic tangent activation function – hereinafter referred to as a *deep FNN with ReLU and Tanh activation*. We deliver the following major contributions:

- 1) We derive the fundamental asymptotic testing performance limits of binary classifiers based on a hinge-loss-trained deep ReLU FNN.
- 2) We conduct extensive computer experiments whose results corroborate our derived asymptotic testing performance limits for deep ReLU FNN.
- 3) We derive the asymptotic testing performance limits of binary classifiers based on a hinge-loss-trained deep FNN with ReLU and Tanh activation.

2. For a regression AI/ML algorithm, the authors of [67] are the first to provide asymptotic and non-asymptotic fundamental testing performance limits for a ReLU FNN-based regression AI/ML algorithm. The authors of [68] derive the asymptotic performance limits on a DL-based text semantic communication system subjected to interference.

- 4) We perform extensive computer experiments whose results validate our derived asymptotic testing performance limits for deep FNN with ReLU and Tanh activation.

The remainder of this paper is organized as follows. Section 2 outlines the prelude and system setup. Section 3 presents the problem formulations. Section 4 documents the derived asymptotic testing performance limits. Section 5 reports on extensive computer experiments. Last, Section 6 underscores our concluding remarks and research outlook.

*Notation:* Scalars, vectors, and matrices are represented by italic, bold lowercase, and bold uppercase letters, respectively. Uppercase italic letters denote random variables. Uppercase calligraphic letters denote events, hypotheses, and sets.  $\mathbb{N}, \mathbb{N}_0, (\mathbb{R}_+)\mathbb{R}, \mathbb{R} \setminus \{0\}, \mathbb{R}^n$ , and  $(\mathbb{R}_+^{m \times n})\mathbb{R}^{m \times n}$  denote the sets of natural numbers, natural numbers including zero, (positive)real numbers, real numbers excluding zero,  $n$ -dimensional real vectors, and  $m \times n$  (positive)real matrices, respectively.  $\sim, :=, \equiv, \mathbf{0}, \mathbf{I}_n, \exp(\cdot)$ , and  $\mathbb{P}(\cdot)$  stand for distributed as, equal by definition, equivalent to, a zero vector/matrix whose dimension will be clear in context, an  $n \times n$  identity matrix, exponential function, and probability, respectively.  $\text{diag}(\cdot)$ ,  $\text{sgn}(\cdot)$ ,  $\max(\cdot, \dots, \cdot)$ ,  $\min(\cdot, \dots, \cdot)$ ,  $\mathcal{N}(\mu, \sigma^2)$ ,  $(\cdot)^\top$ ,  $\mathbb{I}\{\cdot\}$ , and  $|\cdot|$  stand for a diagonal matrix, the sign function, maximum of, minimum of, Gaussian distribution with mean  $\mu$  and variance  $\sigma^2$ , transpose, a (component-wise) indicator function that returns 1 if the argument is true and 0 otherwise, and cardinality, respectively.

$\mathcal{Q}(\cdot)$  denotes the  $\mathcal{Q}$ -function defined for  $x \in \mathbb{R}$  as  $\mathcal{Q}(x) := \frac{1}{\sqrt{2\pi}} \int_x^\infty \exp(-t^2/2)dt$ .  $\arg \min, \cap, \cup, \|\cdot\|, \delta(\cdot)$ , and  $\ln(\cdot)$  stand for the arguments of the minima, the intersection of two sets/events, the union of two sets/events, a vector norm, the Dirac delta function, and the natural logarithm, respectively.  $\mathbb{N}_{\geq k} := \{k, k+1, \dots\}$  denotes the sets of natural numbers greater than or equal to  $k$  with  $k \in \mathbb{N}_0$ . For  $n \in \mathbb{N}_{\geq 1}$ ,  $[n] := \{1, \dots, n\}$ . For  $\mathbf{A} \in \mathbb{R}^{m \times n}$  and  $\mathbf{a} \in \mathbb{R}^n$ ,  $(\mathbf{A})_{i,j}$  and  $(\mathbf{a})_i$  denote the  $(i, j)$ -th element of  $\mathbf{A}$  and the  $i$ -th entry of  $\mathbf{a}$ , respectively. Per the MATLAB<sup>®</sup> syntax,  $\mathbf{A}(i, :)$  denotes the  $i$ -th row of  $\mathbf{A} \in \mathbb{R}^{m \times n}$ . For  $\mathbf{A} \in \mathbb{R}^{m \times n}$  and  $\mathbf{a} \in \mathbb{R}^n$ ,  $\|\mathbf{A}\|_{\ell_0} := |\{(i, j) : (\mathbf{A})_{i,j} \neq 0\}|$ ,  $\|\mathbf{a}\|_\infty := \max_{i=1, \dots, n} |(\mathbf{a})_i|$ , and  $\|\mathbf{A}\|_\infty := \max_{i,j} |(\mathbf{A})_{i,j}|$ . For  $n \in \mathbb{N}_{\geq 2}$ , the horizontal concatenation of  $n$  conformable vectors and matrices is written as  $[\mathbf{a}_1 \ \mathbf{a}_2 \ \dots \ \mathbf{a}_n]$  and  $[\mathbf{A}_1 \ \mathbf{A}_2 \ \dots \ \mathbf{A}_n]$ , respectively.

## 2 PRELUDE AND SYSTEM SETUP

### 2.1 Prelude

**Definition 1 (Definition of FNNs [69, Definition 2.2]).** Let  $K, N_0, N_1, \dots, N_K \in \mathbb{N}$  and  $K \geq 2$ . A FNN  $\Phi$  is a sequence of matrix-vector tuples defined as

$$\Phi := [[\mathbf{W}_1, \mathbf{b}_1], \mathbf{W}_2, \mathbf{b}_2], \dots, [\mathbf{W}_K, \mathbf{b}_K]], \quad (1)$$

where  $\mathbf{W}_k \in \mathbb{R}^{N_k \times N_{k-1}}$  and  $\mathbf{b}_k \in \mathbb{R}^{N_k}$  are the weight matrix of the neuronal connections between the  $k$ -th and  $(k-1)$ -th layers and the  $k$ -th layer's biases given  $N_k$  is the number of neurons in the  $k$ -th layer (the input layer is considered the 0-th layer), respectively. For the  $K$ -layer FNN expressed by (1),  $\mathcal{N}(\Phi) := \sum_{k=0}^K N_k$ ,  $\mathcal{M}(\Phi) := \sum_{k=1}^K (\|\mathbf{W}_k\|_{\ell_0} + \|\mathbf{b}_k\|_{\ell_0})$ ,  $\mathcal{W}(\Phi) := \max_{k=0, \dots, K} N_k$ , and  $\mathcal{B}(\Phi) := \max_{k \in [K]} \{\|\mathbf{W}_k\|_\infty, \|\mathbf{b}_k\|_\infty\}$

define the total number of neurons, the network connectivity, the maximum width, and the maximum absolute value of the weights, respectively. For an input  $\mathbf{x} \in \mathbb{R}^{N_0}$  and an element-wise activation function  $\rho(\cdot)$ , an FNN map  $\Phi : \mathbb{R}^{N_0} \rightarrow \mathbb{R}^{N_K}$  is defined as  $\Phi(\mathbf{x}) = \mathbf{x}_K$ , where  $\mathbf{x}_K$  is obtained recursively as

$$\mathbf{x}_0 := \mathbf{x}; \quad \mathbf{x}_k := \rho(\mathbf{W}_k \mathbf{x}_{k-1} + \mathbf{b}_k), \quad \forall k \in [K-1] \quad (2a)$$

$$\mathbf{x}_K := \mathbf{W}_K \mathbf{x}_{K-1} + \mathbf{b}_K, \quad (2b)$$

where  $\rho(\mathbf{y}) = [\rho(y_1), \dots, \rho(y_m)]^\top$  for  $\mathbf{y} = [y_1, \dots, y_m]^\top \in \mathbb{R}^m$ . For  $\rho(y_i) := \max(y_i, 0)$ , the FNN in (1) is known as a ReLU FNN. This type of FNN is often termed a deep ReLU neural network when  $K$  is very large. When  $N_k, k \in [K]$ , is very large (often a polynomial order of the input number of neurons and the data points [50], [51]), the FNN is usually termed an over-parameterized ReLU neural network if  $K$  is small and an over-parameterized deep ReLU neural network if  $K$  is very large.

**Definition 2 (FNNs with dual activation functions [63]).** Let  $t \in \mathbb{N}_0, n \in \mathbb{N}$ , and  $K \in \mathbb{N}_{\geq 2}$ . Let  $N_1, N_k, N_{k-1} \in \mathbb{N}_{\geq 2}$  for  $k \in [K]$ . Assume an FNN training over  $\mathcal{D} := \{(x_n, y_n)\}_{n=1}^N$  given  $x_n$  and  $y_n \in \{-1, 1\}$  are the  $n$ -th input generated per (4) and the  $n$ -th label, respectively. For a  $K$ -layer FNN with dual activation functions – denoted by  $\varphi(\cdot)$  and  $\phi(\cdot)$  – and  $N_k$  neurons in its  $k$ -th layer, the network prediction during the  $t$ -th iteration is obtained as<sup>3</sup>

$$\mathbf{y}_{1,n}^{(t)} = \varphi(\mathbf{w}_1^{(t)} x_n) \quad (3a)$$

$$\mathbf{y}_{k,n}^{(t)} = \varphi(\mathbf{W}_k^{(t)} \mathbf{y}_{k-1,n}^{(t)}), \quad \forall k \in \{2, \dots, K-1\} \quad (3b)$$

$$\mathbf{y}_{K,n}^{(t)} = \phi(\mathbf{w}_K^{(t)} \mathbf{y}_{K-1,n}^{(t)}), \quad (3c)$$

where  $\varphi(\mathbf{x}) = [\varphi(x_1), \dots, \varphi(x_m)]^\top \in \mathbb{R}^m$  for  $\mathbf{x} = [x_1, \dots, x_m]^\top \in \mathbb{R}^m$ ;  $\mathbf{w}_1^{(t)} \in \mathbb{R}^{N_1}$ ,  $\mathbf{W}_k^{(t)} \in \mathbb{R}^{N_k \times N_{k-1}}$ , and  $(\mathbf{w}_K^{(t)})^\top \in \mathbb{R}^{N_{K-1}}$ ;  $\mathbf{y}_{1,n}^{(t)} \in \mathbb{R}^{N_1}$ ,  $\mathbf{y}_{k,n}^{(t)} \in \mathbb{R}^{N_k}$ , and  $y_{K,n}^{(t)} \in \mathbb{R}$  are the first,  $k$ -th, and  $K$ -th layers' outputs, respectively, at the  $t$ -th stochastic gradient descent (SGD) iteration<sup>4</sup> in response to the  $n$ -th training input drawn from  $\mathcal{D}$ ; and  $\phi(\mathbf{y}) = [\phi(y_1), \dots, \phi(y_n)]^\top \in \mathbb{R}^n$  for  $\mathbf{y} = [y_1, \dots, y_n]^\top \in \mathbb{R}^n$ .

**Remark 1.** For a ReLU FNN,  $\varphi(x) = \rho(x) := \max(0, x)$  and  $\phi(x) = x$  for  $x \in \mathbb{R}$ . For an FNN with ReLU and Tanh activation,  $\varphi(x) = \rho(x)$  and  $\phi(x) = \tanh(x)$  for  $x \in \mathbb{R}$ .

We now proceed with a generic DL-based binary classification problem to investigate the fundamental limits of DL-based classification algorithms as applied to wireless communications and networking, signal processing, neuroscience, and quantum communications and networking.

### 2.2 System Setup

Consider a generic DL-based binary classification problem on hypotheses  $\mathcal{H}_{-1}$  and  $\mathcal{H}_1$  regarding the input datum  $x_n$  defined through binary hypothesis testing as

$$x_n = \begin{cases} f(\xi_n) + z_n & : \mathcal{H}_{-1} \\ f(\beta_n) + z_n & : \mathcal{H}_1, \end{cases} \quad (4)$$

3. As the biases can be subsumed by a linear model expressed by a non-zero weight matrix and an input equal to 1, they are discarded [63].

4. The  $t$ -th iteration accounts for the forward propagation of all the inputs of a mini-batch randomly chosen prior to forward-propagation.

where  $n \in \mathbb{N}$  and  $x_n \in \mathbb{R}$ ;  $f$  is an unknown generic function whose noisy outputs give rise to  $x_n$ ;  $\xi_n, \beta_n \in \mathbb{R}$  for  $\xi_n \neq \beta_n$  are unknown data-generating input variables that are independent of  $z_n \in \mathbb{R}$ ; and  $z_n \sim \mathcal{N}(0, \sigma^2)$  is additive white Gaussian noise (AWGN) with zero mean and variance. To solve the binary pattern classification problem in (4), we consider a deep FNN-based binary classifier trained using a training set  $\mathcal{D} := \{(x_n, y_n)\}_{n=1}^N$  – given  $x_n$  is the  $n$ -th input generated via (4) and  $y_n \in \{-1, 1\}$  is the  $n$ -th label – and hinge loss per the back-propagation algorithm.<sup>5</sup>

Let  $(\mathbf{w}_K^{(t)})^\top \in \mathbb{R}^{2H}$ ,  $\mathbf{W}_{K-k}^{(t)} \in \mathbb{R}^{2H \times 2H} \forall k \in [K-2]$ , and  $\mathbf{w}_1^{(t)} \in \mathbb{R}^{2H}$  be the weight matrices of the  $K$ -th layer, the  $k$ -th layer, and the first layer of a *bi-asless* deep ReLU FNN under training during the  $t$ -th iteration, respectively. During this iteration,  $\Phi^{(t)} := [[\mathbf{w}_1^{(t)}, \mathbf{0}], [\mathbf{W}_2^{(t)}, \mathbf{0}], \dots, [\mathbf{W}_{K-1}^{(t)}, \mathbf{0}], [\mathbf{w}_K^{(t)}, \mathbf{0}]]$  defines a deep ReLU FNN under training and whose output is given by

$$\Phi^{(t)}(x_n) := \mathbf{w}_K^{(t)} \mathbf{y}_{K-1,n} \in \mathbb{R}, \quad (5)$$

where, for  $\Sigma_{1,n}^{(t)} = \text{diag}(\mathbb{I}\{\mathbf{w}_1^{(t)} x_n \geq 0\}) \in \{0, 1\}^{2H \times 2H}$  and  $\Sigma_{k,n}^{(t)} = \text{diag}(\mathbb{I}\{\mathbf{W}_k^{(t)} (\prod_{l=1}^{k-2} \Sigma_{k-l,n}^{(t)} \mathbf{W}_{k-l}^{(t)}) \Sigma_{1,n}^{(t)} \mathbf{w}_1^{(t)} x_n \geq 0\}) \in \{0, 1\}^{2H \times 2H}$  [51],

$$\mathbf{y}_{K-1,n} = \left( \prod_{k=1}^{K-2} \Sigma_{K-k,n}^{(t)} \mathbf{W}_{K-k}^{(t)} \right) \Sigma_{1,n}^{(t)} \mathbf{w}_1^{(t)} x_n \in \mathbb{R}_+^{2H}. \quad (6)$$

Note that  $\mathbf{y}_{K-1,n}^{(t)}$  is the output of the  $(K-1)$ -th deep ReLU FNN layer during the  $t$ -th iteration.

The output of a deep FNN with ReLU and Tanh activation – denoted by  $\check{\Phi}^{(t)}$  – is equated as

$$\check{\Phi}^{(t)}(x_n) := \tanh(\check{\mathbf{w}}_K^{(t)} \check{\mathbf{y}}_{K-1,n}^{(t)}) \in \mathbb{R}, \quad (7)$$

where  $\check{\Phi}^{(t)} := [[\check{\mathbf{w}}_1^{(t)}, \mathbf{0}], [\check{\mathbf{W}}_2^{(t)}, \mathbf{0}], \dots, [\check{\mathbf{W}}_{K-1}^{(t)}, \mathbf{0}], [\check{\mathbf{w}}_K^{(t)}, \mathbf{0}]]$  given  $(\check{\mathbf{w}}_K^{(t)})^\top \in \mathbb{R}^{2H}$ ,  $\check{\mathbf{W}}_{K-k}^{(t)} \in \mathbb{R}^{2H \times 2H}$  for all  $k \in [K-2]$ , and  $\check{\mathbf{w}}_1^{(t)} \in \mathbb{R}^{2H}$ , and  $\check{\mathbf{y}}_{K-1,n}^{(t)}$  is the output of the  $(K-1)$ -th deep FNN layer during the  $t$ -th iteration, which is given by

$$\check{\mathbf{y}}_{K-1,n}^{(t)} = \left( \prod_{k=1}^{K-2} \check{\Sigma}_{K-k,n}^{(t)} \check{\mathbf{W}}_{K-k}^{(t)} \right) \check{\Sigma}_{1,n}^{(t)} \check{\mathbf{w}}_1^{(t)} x_n \in \mathbb{R}_+^{2H}, \quad (8)$$

where  $\check{\Sigma}_{k,n}^{(t)} = \text{diag}(\mathbb{I}\{\check{\mathbf{W}}_k^{(t)} (\prod_{l=1}^{k-2} \check{\Sigma}_{k-l,n}^{(t)} \check{\mathbf{W}}_{k-l}^{(t)}) \check{\Sigma}_{1,n}^{(t)} \check{\mathbf{w}}_1^{(t)} x_n \geq 0\}) \in \{0, 1\}^{2H \times 2H}$  and  $\check{\Sigma}_{1,n}^{(t)} = \text{diag}(\mathbb{I}\{\check{\mathbf{w}}_1^{(t)} x_n \geq 0\}) \in \{0, 1\}^{2H \times 2H}$ . Minimizing the training loss of this deep FNN and the mentioned deep ReLU FNN follows via (7) and (5), respectively, on a mini-batch-by-mini-batch basis.

After forward-propagating the  $t$ -th mini-batch  $\mathcal{B}^{(t)}$  sampled randomly from  $\mathcal{D}$ , the training loss exhibited by the aforementioned deep ReLU FNN and deep FNN – trained using hinge loss  $\ell(t, y) := \max(0, 1 - ty)$  – is defined as

$$L_{\mathcal{B}^{(t)}}(\mathbf{W}^{(t)}) := B^{-1} \sum_{i \in \mathcal{B}^{(t)}} \ell(y_i, f_{\mathbf{W}^{(t)}}(x_i)), \quad (9)$$

5. The derivation of the back-propagation algorithm (using square loss) is often documented using scalar calculus for an FNN equipped with the same activation function throughout all its layers [63, Ch. 4]. For completeness and clarity, we employ *matrix calculus* to derive the update rules for back-propagation w.r.t. hinge loss and SGD for FNNs with dual activation functions, as detailed in [70, Appendix A, p. 45-52].

where  $B := |\mathcal{B}^{(t)}|$ ,  $\mathbf{W}^{(t)}$  is the concatenated weights of all layers, and  $f_{\mathbf{W}^{(t)}}(x_n) = \Phi^{(t)}(x_n)$  per (5) or  $f_{\mathbf{W}^{(t)}}(x_n) = \check{\Phi}^{(t)}(x_n)$  per (7). The deep FNNs' overall training error over  $\mathcal{D}$  can be expressed as [71]

$$R_{\mathcal{D}}(\mathbf{W}^{(t)}) := N^{-1} \sum_{n=1}^N \mathbb{I}\{y_n \neq \text{sgn}(f_{\mathbf{W}^{(t)}}(x_n))\}. \quad (10)$$

To minimize (10), training of DL-based binary classifiers is conducted using the back-propagation algorithm to solve  $\mathbf{W}^* := \sum_{t \in \mathbb{N}, \mathcal{B}^{(t)} \subset \mathcal{D}} \arg \min_{\mathbf{W}^{(t)}} L_{\mathcal{B}^{(t)}}(\mathbf{W}^{(t)})$  while learning deep models that generalize better. To reveal the fundamental limits of such DL-based binary classification, we move on to the following problem formulation.

### 3 PROBLEM FORMULATION

#### 3.1 Problems for ReLU FNNs-Based Binary Classifiers

Let  $\Phi^{(T)} := [[\mathbf{w}_1^{(T)}, \mathbf{0}], [\mathbf{W}_2^{(T)}, \mathbf{0}], \dots, [\mathbf{W}_{K-1}^{(T)}, \mathbf{0}], [\mathbf{w}_K^{(T)}, \mathbf{0}]]$  be a deep ReLU FNN trained using hinge loss and SGD, SGD with momentum, RMSProp, or Adam after being initialized by a Gaussian initializer such as LeCun normal or He normal [70, Definition 10]. Note that  $\mathbf{w}_1^{(T)} = \mathbf{w}_1^{(0)} + \sum_{t=0}^{T-1} \Delta \mathbf{w}_1^{(t)} \in \mathbb{R}^{2H}$ ,  $\mathbf{W}_k^{(T)} = \mathbf{W}_k^{(0)} + \sum_{t=0}^{T-1} \Delta \mathbf{W}_k^{(t)}$ , and

$$\mathbf{w}_K^{(T)} = \mathbf{w}_K^{(0)} + \sum_{t=0}^{T-1} \Delta \mathbf{w}_K^{(t)} \in \mathbb{R}^{1 \times 2H}, \quad (11)$$

where  $T \in \mathbb{N}$ ;  $\mathbf{w}_1^{(0)}$ ,  $\mathbf{W}_k^{(0)}$ , and  $\mathbf{w}_K^{(0)}$  are weight matrices/vectors initialized with Gaussian initializers;  $\Delta \mathbf{w}_1^{(t)}$ ,  $\Delta \mathbf{W}_k^{(t)}$ , and  $\Delta \mathbf{w}_K^{(t)}$  are the  $t$ -th back-propagated error matrices/vectors. As to a collected weight matrix  $\mathbf{W}^{(T)} := [\mathbf{w}_1^{(T)} \mathbf{W}_2^{(T)} \dots \mathbf{W}_{K-1}^{(T)} (\mathbf{w}_K^{(T)})^\top]$  of all the layers' trained weights, the testing error over the testing set  $\mathcal{T} := \{(x_n, y_n)\}_{n=N+1}^{N+\tilde{N}}$  – given that  $x_n$  is the  $n$ -th input generated via (4) and  $y_n \in \{-1, 1\}$  is the  $n$ -th label for all  $n \in \{N+1, \dots, N+\tilde{N}\}$  – can be defined as

$$R_{\mathcal{T}}(\mathbf{W}^{(T)}) := \tilde{N}^{-1} \sum_{n=N+1}^{N+\tilde{N}} \mathbb{I}\{y_n \neq \text{sgn}(\Phi^{(T)}(x_n))\}, \quad (12)$$

where  $\tilde{N} := |\mathcal{T}|$ . W.r.t. the right-hand side (RHS) of (12), the underneath lemma ensues.

**Lemma 1.** For  $y_n \in \{-1, 1\}$  and  $n \in \mathbb{N}$ ,

$$\mathbb{I}\{y_n \neq \text{sgn}(\Phi^{(T)}(x_n))\} \equiv \mathbb{I}\{y_n \Phi^{(T)}(x_n) \leq 0\}. \quad (13)$$

*Proof.* We provide the proof in [70, Appendix B, p. 53].

Substituting (13) in the RHS of (12) gives

$$R_{\mathcal{T}}(\mathbf{W}^{(T)}) = \tilde{N}^{-1} \sum_{n=N+1}^{N+\tilde{N}} \mathbb{I}\{y_n \Phi^{(T)}(x_n) \leq 0\}. \quad (14)$$

Hence, the average probability of misclassification error  $\bar{P}_e$  manifested by  $\Phi^{(T)}$  becomes

$$\bar{P}_e = \tilde{N}^{-1} \sum_{n=N+1}^{N+\tilde{N}} \mathbb{P}(y_n \Phi^{(T)}(x_n) \leq 0). \quad (15)$$

As for (15), the probability of point misclassification error  $P_e$  manifested by  $\Phi^{(T)}$  equates to

$$P_e = \mathbb{P}(y_n \Phi^{(T)}(x_n) \leq 0). \quad (16)$$

The RHS of (16) is simplified – as done in [70, eq. (39b)] to [70, (40d)] – using the *law of total probability* [70, Law 1] for equally likely labels that  $\mathbb{P}(y_n = \pm 1) = 1/2$ :

$$P_e = \frac{1}{2} [\mathbb{P}(\Phi^{(T)}(x_n) > 0 | \mathcal{H}_{-1}) + \mathbb{P}(\Phi^{(T)}(x_n) < 0 | \mathcal{H}_1)]. \quad (17)$$

We formulate the following problems w.r.t.  $\mathbf{y}_{K-1,n}^{(T)}$  defined via (6) and  $P_e$  given by (17).

**Problem 1.** Characterize  $\lim_{(\|\mathbf{y}_{K-1,n}^{(T)}\| \|\mathcal{H}_{-1}\|, \|\mathbf{y}_{K-1,n}^{(T)}\| \|\mathcal{H}_1\|) \rightarrow (\infty, \infty)} P_e$ .

**Problem 2.** Quantify  $\lim_{(\|\mathbf{y}_{K-1,n}^{(T)}\| \|\mathcal{H}_{-1}\|, \|\mathbf{y}_{K-1,n}^{(T)}\| \|\mathcal{H}_1\|) \rightarrow (0, \infty)} P_e$ .

Problems 1&2 are novel in the sense that a problem solver should address the interpretability of a trained deep ReLU FNN model while also circumventing the random gradients (with unknown distribution) that were back-propagated during training.

### 3.2 Problems for Binary Classifiers based on FNNs with ReLU and Tanh Activation

Let  $\check{\Phi}^{(T)} := [[\check{\mathbf{w}}_1^{(T)}, \mathbf{0}], [\check{\mathbf{W}}_2^{(T)}, \mathbf{0}], \dots, [\check{\mathbf{W}}_{K-1}^{(T)}, \mathbf{0}], [\check{\mathbf{w}}_K^{(T)}, \mathbf{0}]]$  be a deep FNN trained using hinge loss and SGD, SGD with momentum, RMSProp, or Adam after being initialized with a Gaussian initializer such as LeCun normal or He normal. Note that  $\check{\mathbf{w}}_1^{(T)} = \check{\mathbf{w}}_1^{(0)} + \sum_{t=0}^{T-1} \Delta \check{\mathbf{w}}_1^{(t)} \in \mathbb{R}^{2H}$ ,  $\check{\mathbf{W}}_k^{(T)} = \check{\mathbf{W}}_k^{(0)} + \sum_{t=0}^{T-1} \Delta \check{\mathbf{W}}_k^{(t)} \in \mathbb{R}^{2H \times 2H}$ , and

$$\check{\mathbf{w}}_K^{(T)} = \check{\mathbf{w}}_K^{(0)} + \sum_{t=0}^{T-1} \Delta \check{\mathbf{w}}_K^{(t)} \in \mathbb{R}^{1 \times 2H}, \quad (18)$$

where  $\check{\mathbf{w}}_1^{(0)}$ ,  $\check{\mathbf{W}}_k^{(0)}$ , and  $\check{\mathbf{w}}_K^{(0)}$  are weight matrices/vectors initialized with Gaussian initializers;  $\Delta \check{\mathbf{w}}_1^{(t)}$ ,  $\Delta \check{\mathbf{W}}_k^{(t)}$ , and  $\Delta \check{\mathbf{w}}_K^{(t)}$  are the  $t$ -th back-propagated error matrices/vectors.

Following (17), the probability of point misclassification error  $\check{P}_e$  manifested by  $\check{\Phi}^{(T)}$  is given by

$$\check{P}_e = \frac{1}{2} [\mathbb{P}(\check{\Phi}^{(T)}(x_n) > 0 | \mathcal{H}_{-1}) + \mathbb{P}(\check{\Phi}^{(T)}(x_n) < 0 | \mathcal{H}_1)]. \quad (19)$$

We formulate the following problems for (19) w.r.t.  $\check{\mathbf{y}}_{K-1,n}^{(T)}$  which is defined via (8), and  $\check{P}_e$  given by (19).

**Problem 3.** Determine  $\lim_{(\|\check{\mathbf{y}}_{K-1,n}^{(T)}\| \|\mathcal{H}_{-1}\|, \|\check{\mathbf{y}}_{K-1,n}^{(T)}\| \|\mathcal{H}_1\|) \rightarrow (\infty, \infty)} \check{P}_e$ .

**Problem 4.** Derive  $\lim_{(\|\check{\mathbf{y}}_{K-1,n}^{(T)}\| \|\mathcal{H}_{-1}\|, \|\check{\mathbf{y}}_{K-1,n}^{(T)}\| \|\mathcal{H}_1\|) \rightarrow (0, \infty)} \check{P}_e$ .

Problems 3&4 are also novel in the sense that a problem solver must tackle the interpretability of a trained deep FNN model with ReLU and Tanh activation while also circumventing the random gradients (with unknown distribution) that were back-propagated during training.

## 4 ASYMPTOTIC TESTING PERFORMANCE LIMITS

### 4.1 Performance Limits of Binary Classifiers that are Based on Deep ReLU FNNs

The asymptotic testing performance limits of  $\Phi^{(T)}$  follow.

**Theorem 1.** Consider a (deep) ReLU FNN  $\Phi^{(T)} := [[\mathbf{w}_1^{(T)}, \mathbf{0}], [\mathbf{W}_2^{(T)}, \mathbf{0}], \dots, [\mathbf{W}_{K-1}^{(T)}, \mathbf{0}], [\mathbf{w}_K^{(T)}, \mathbf{0}]]$  – such that  $\mathbf{w}_K^{(T)} \in \mathbb{R}^{1 \times 2H}$ ,  $\mathbf{W}_{K-k}^{(T)} \in \mathbb{R}^{2H \times 2H}$  for all  $k \in [K-2]$ , and  $\mathbf{w}_1^{(T)} \in \mathbb{R}^{2H}$  – trained over  $\mathcal{D} := \{(x_n, y_n)\}_{n=1}^N$  using the settings of Sec. 3.1, and to be tested over  $\mathcal{T} := \{(x_n, y_n)\}_{n=N+1}^{N+\tilde{N}}$  given  $H, K, N, \tilde{N}, T \in \mathbb{N}$ . For  $N, \tilde{N}, T, K \geq 2$ , and  $H < \infty$ :

$$\lim_{\|\mathbf{y}_{K-1,n}^{(T)}\| \rightarrow \infty} P_e \leq 1/2 \quad (20a)$$

$$\lim_{(\|\mathbf{y}_{K-1,n}^{(T)}\| \|\mathcal{H}_{-1}\|, \|\mathbf{y}_{K-1,n}^{(T)}\| \|\mathcal{H}_1\|) \rightarrow (0, \infty)} P_e \leq 1/2, \quad (20b)$$

where (20a) and (20b) are valid for all  $n \in \{N+1, \dots, N+\tilde{N}\}$ .

*Proof.* The proof is given in the supplementary material.

**Remark 2.** Theorem 1 is valid for any training/testing dataset size, network depth, or (finite) network width, since (20a) and (20b) are valid for any  $N, \tilde{N}, T, K \geq 2$ , and  $H < \infty$ .

**Remark 3.** Theorem 1 applies to any binary classification AI/ML problem solved using a (deep) ReLU FNN that has been trained with hinge loss and SGD, SGD with momentum, RMSProp, or Adam after being initialized with a Gaussian initializer such as LeCun normal or He normal, because it does not make any assumptions w.r.t. the input hypotheses.

**Remark 4.** If  $\|\mathbf{y}_{K-1,n}^{(T)}\| \rightarrow \infty$  or  $(\|\mathbf{y}_{K-1,n}^{(T)}\| \|\mathcal{H}_{-1}\|, \|\mathbf{y}_{K-1,n}^{(T)}\| \|\mathcal{H}_1\|) \rightarrow (0, \infty)$ , the exhibited probability of misclassification error will be upper bounded by 1/2, where the binary classifier would be in a coin-tossing mode.

### 4.2 Performance Limits of Binary Classifiers based on FNNs with ReLU and Tanh Activation

The asymptotic testing performance limits of  $\check{\Phi}^{(T)}$  ensue.

**Theorem 2.** Consider a (deep) FNN with ReLU and Tanh activation  $\check{\Phi}^{(T)} := [[\check{\mathbf{w}}_1^{(T)}, \mathbf{0}], [\check{\mathbf{W}}_2^{(T)}, \mathbf{0}], \dots, [\check{\mathbf{W}}_{K-1}^{(T)}, \mathbf{0}], [\check{\mathbf{w}}_K^{(T)}, \mathbf{0}]]$  – such that  $\check{\mathbf{w}}_K^{(T)} \in \mathbb{R}^{1 \times 2H}$ ,  $\check{\mathbf{W}}_{K-k}^{(T)} \in \mathbb{R}^{2H \times 2H} \forall k \in [K-2]$ , and  $\check{\mathbf{w}}_1^{(T)} \in \mathbb{R}^{2H}$  – trained over  $\mathcal{D} := \{(x_n, y_n)\}_{n=1}^N$  per the settings of Sec. 3.2, and to be tested over  $\mathcal{T} := \{(x_n, y_n)\}_{n=N+1}^{N+\tilde{N}}$  given  $H, K, N, \tilde{N}, T \in \mathbb{N}$ . For  $N, \tilde{N}, T, K \geq 2$  and  $H < \infty$ :

$$\lim_{\|\check{\mathbf{y}}_{K-1,n}^{(T)}\| \rightarrow \infty} \check{P}_e \leq 1/2 \quad (21a)$$

$$\lim_{(\|\check{\mathbf{y}}_{K-1,n}^{(T)}\| \|\mathcal{H}_{-1}\|, \|\check{\mathbf{y}}_{K-1,n}^{(T)}\| \|\mathcal{H}_1\|) \rightarrow (0, \infty)} \check{P}_e \leq 1/2, \quad (21b)$$

where (21a) and (21b) are true for all  $n \in \{N+1, \dots, N+\tilde{N}\}$ .

*Proof.* The proof is provided in the supplementary material.

**Remark 5.** Theorem 2 is valid for any training/testing dataset size, network depth, or (finite) network width, because (21a) and (21b) are valid for any  $N, \tilde{N}, T, K \geq 2$ , and  $H < \infty$ .

SNR [in dB]	Optimal detector	ReLU FNN-based BPSK detector (K, H) = (3, 3)			ReLU FNN-based BPSK detector (K, H) = (3, 9)		
$\gamma_b$ [dB]	$\mathcal{Q}(\sqrt{2\gamma_b})$	All-SNR-T	High-SNR-T	Low-SNR-T	All-SNR-T	High-SNR-T	Low-SNR-T
0	0.0786	0.56448001	0.75902	0.56411999	0.56411999	0.59154001	0.56402001
5	0.0060	0.50569999	0.57170001	0.50566	0.50566	0.51100001	0.50564
10	$3.8721 \times 10^{-6}$	0.50075999	0.50128001	0.50075999	0.50075999	0.50075999	0.50075999
15	$9.1240 \times 10^{-16}$	0.50338	0.50338	0.50338	0.50338	0.50338	0.50338
20	$1.0442 \times 10^{-45}$	0.49835998	0.49835998	0.49835998	0.49835998	0.49835998	0.49835998
25	$7.3070 \times 10^{-140}$	0.49908	0.49908	0.49908	0.49908	0.49908	0.49908
30	0	0.49677998	0.49677998	0.49677998	0.49677998	0.49677998	0.49677998
35	0	0.50049999	0.50049999	0.50049999	0.50049999	0.50049999	0.50049999

TABLE 1: Numerical results I on bit error rate manifested by optimal BPSK detector and ReLU FNN-based BPSK detectors.

**Remark 6.** Theorem 2 is applicable to any binary classification AI/ML problem solved using a deep FNN with ReLU and Tanh activation that has been trained with hinge loss and SGD, SGD with momentum, RMSProp, or Adam after being initialized with a Gaussian initializer such as LeCun normal or He normal, since it does not make any assumptions w.r.t. the input hypotheses.

**Remark 7.** If  $\|\tilde{\mathbf{y}}_{K-1,n}^{(T)}\| \rightarrow \infty$  or  $(\|\tilde{\mathbf{y}}_{K-1,n}^{(T)}\|, \|\tilde{\mathbf{y}}_{K-1,n}^{(T)}\|_{\mathcal{H}_1}) \rightarrow (0, \infty)$ , the manifested probability of misclassification error will be upper bounded by 1/2, where the binary classifier would be in a coin-tossing mode.

## 5 COMPUTER EXPERIMENTS

### 5.1 DL-Based Binary Classification Settings

In view of the generic binary hypothesis testing of (4), we opt for a classical optimum detection problem involving a binary phase shift keying (BPSK) signal received over an AWGN channel. For a received AWGN-contaminated BPSK signal having a bit duration of  $T_s$ , we consider the received passband signal is down-converted to the received baseband signal, denoted by  $r(t)$ , which is sampled per the Nyquist rate  $f_s = 1/T_s$  to produce the sampled baseband signal  $r[n] := r(nT_s)$  given for  $n \in \mathbb{N}$  by

$$r[n] = \begin{cases} -\sqrt{\mathcal{E}_b} + z[n] & : \mathcal{H}_{-1} \\ \sqrt{\mathcal{E}_b} + z[n] & : \mathcal{H}_1, \end{cases} \quad (22)$$

where  $\mathcal{E}_b$  is the transmitted energy per bit;  $s_0 = -\sqrt{\mathcal{E}_b}$  and  $s_1 = \sqrt{\mathcal{E}_b}$  are the equally likely samples of the transmitted BPSK signal pertaining to bit 0 and bit 1, respectively;  $z[n] \sim \mathcal{N}(0, N_0/2)$  denotes the AWGN samples obtained from the AWGN process  $z(t)$  as  $z[n] := z(nT_s)$ , where  $N_0$  is the power spectral density of the noise; and  $\mathcal{H}_{-1}$  and  $\mathcal{H}_1$  are hypotheses corresponding to the transmission of  $s_0$  and  $s_1$ , respectively. As to the problem in (22), an optimum BPSK detector's manifested probability of bit error ( $P_e$ ) is given by  $\tilde{P}_e = \mathcal{Q}(\sqrt{2\gamma_b})$ , as we proved in [70, Appendix E, p. 65-68], where  $\gamma_b$  is the signal-to-noise ratio (SNR) per bit. This was used as a baseline for our computer experiments assessing the performance of DL-based BPSK detectors.

### 5.2 Materials and Methods

After using MATLAB® to generate our training and testing sets, our computer experiments were carried out on the NIST GPU cluster named *Enki* using Keras with TensorFlow as a backend. Our training sets  $\mathcal{D}_1$  and  $\mathcal{D}_2$  were

generated by combining the training data generated for  $\gamma_b \in \{0, 5, 10, 15, 20, 25, 30, 35\}$  dB. For  $\gamma_b^i = 5(i-1)$  dB and  $i \in [8]$ , we generated training sets  $\mathcal{D}_1^i$  and  $\mathcal{D}_2^i$  made of  $2 \times 10^5$  inputs equal to the received baseband signal samples produced at  $\gamma_b^i$  and equally likely labels chosen from  $\{-1, 1\}$  as  $\mathcal{D}_1^i := \{(x_n^i, y_n^i)\}_{n=1}^{200,000}$  and  $\mathcal{D}_2^i := \{(x_n^i, y_n^i)\}_{n=1}^{200,000}$  such that  $x_n^i := r[n]_{\gamma_b=\gamma_b^i}$  for  $r[n]$  defined in (22),  $y_n^i \in \{-1, 1\}$ ,  $x_{\tilde{n}}^i := r[\tilde{n}]_{\gamma_b=\gamma_b^i}$  for  $r[\tilde{n}]$  defined via (22), and  $y_{\tilde{n}}^i \in \{-1, 1\}$ . For the generation of  $x_{\tilde{n}}^i := r[\tilde{n}]_{\gamma_b=\gamma_b^i}$  and  $x_n^i := r[n]_{\gamma_b=\gamma_b^i}$  w.r.t.  $\gamma_b^i = \mathcal{E}_b^i/N_0$ , we set  $N_0 = 1$  W/Hz such that  $\gamma_b^i = \mathcal{E}_b^i$ ,  $z[n] \sim \mathcal{N}(0, 1/2)$ , and  $z[\tilde{n}] \sim \mathcal{N}(0, 1/2)$ . We used these settings to generate  $\mathcal{D}_1^i$  and  $\mathcal{D}_2^i$  – for all  $i \in [8]$  – and formed  $\mathcal{D}_1$  and  $\mathcal{D}_2$  as  $\mathcal{D}_1 := \{\mathcal{D}_1^1 \cup \mathcal{D}_1^2 \cup \dots \cup \mathcal{D}_1^7 \cup \mathcal{D}_1^8\}$  and  $\mathcal{D}_2 := \{\mathcal{D}_2^1 \cup \mathcal{D}_2^2 \cup \dots \cup \mathcal{D}_2^7 \cup \mathcal{D}_2^8\}$ , respectively. Similarly, we generated a testing set  $\mathcal{T}$  as  $\mathcal{T} := \{\mathcal{T}^1 \cup \mathcal{T}^2 \cup \dots \cup \mathcal{T}^7 \cup \mathcal{T}^8\}$  for  $\mathcal{T}^i$ ,  $i \in [8]$ , being the testing set generated at SNR  $\gamma_b^i$  such that  $\mathcal{T}^i := \{(x_n^i, y_n^i)\}_{n=200,001}^{250,000}$  for  $x_n^i := r[n]_{\gamma_b=\gamma_b^i}$ ,  $y_n^i \in \{-1, 1\}$ , and  $\gamma_b^i = 5(i-1)$  dB. We then uploaded  $\mathcal{T}$ ,  $\mathcal{D}_1$ , and  $\mathcal{D}_2$  into Enki and implemented three training strategies, namely all SNR training (All-SNR-T), high SNR training (High-SNR-T), and low SNR training (Low-SNR-T).

For All-SNR-T, we formed a training and validation set  $\mathcal{D}$  as  $\mathcal{D} = \mathcal{D}_1$ . For High-SNR-T, we generated a training and validation set  $\mathcal{D}_{\text{high}}$  as  $\mathcal{D}_{\text{high}} = \mathcal{D}_{1,\text{high}} \cup \mathcal{D}_{2,\text{high}}$ , where  $\mathcal{D}_{1,\text{high}} := \{\mathcal{D}_1^5 \cup \mathcal{D}_1^6 \cup \mathcal{D}_1^7 \cup \mathcal{D}_1^8\}$ ,  $\mathcal{D}_{2,\text{high}} := \{\mathcal{D}_2^5 \cup \mathcal{D}_2^6 \cup \mathcal{D}_2^7 \cup \mathcal{D}_2^8\}$ , and  $|\mathcal{D}_{1,\text{high}}| = |\mathcal{D}|$ . For Low-SNR-T, we created a training and validation set  $\mathcal{D}_{\text{low}}$  as  $\mathcal{D}_{\text{low}} = \mathcal{D}_{1,\text{low}} \cup \mathcal{D}_{2,\text{low}}$ , where  $\mathcal{D}_{1,\text{low}} := \{\mathcal{D}_1^1 \cup \mathcal{D}_1^2 \cup \mathcal{D}_1^3 \cup \mathcal{D}_1^4\}$ ,  $\mathcal{D}_{2,\text{low}} := \{\mathcal{D}_2^1 \cup \mathcal{D}_2^2 \cup \mathcal{D}_2^3 \cup \mathcal{D}_2^4\}$ , and  $|\mathcal{D}_{1,\text{low}}| = |\mathcal{D}|$ . Using  $\mathcal{D}_{\text{low}}$ ,  $\mathcal{D}_{\text{high}}$ , and  $\mathcal{D}$ , we executed exhaustive training that led to the optimized (hyper)parameters of [70, Tables VI&VII] for the best performing ReLU FNN models and FNN models with ReLU and Tanh activation, respectively. Besides, we used four KERAS callbacks : TensorBoard, ModelCheckpoint, EarlyStopping, and ReduceLROnPlateau [72, Ch. 7]. EarlyStopping and ReduceLROnPlateau were set to have patience over 20 and 40 epochs, respectively. ReduceLROnPlateau was set to reduce the learning rate by 0.5 for every 20 epochs that led to performance stagnation. Finally, we tested the BPSK detection performance of trained (deep) ReLU FNNs and (deep) FNNs with ReLU and Tanh activation by varying  $(K, H)$  for each testing SNR, leading to the results reported in Sections 5.3 and 5.4.

SNR [in dB]	Optimal detector	ReLU FNN-based BPSK detector ( $K, H$ ) = (7, 7)			ReLU FNN-based BPSK detector ( $K, H$ ) = (7, 14)		
$\gamma_b$ [dB]	$\mathcal{Q}(\sqrt{2\gamma_b})$	All-SNR-T	High-SNR-T	Low-SNR-T	All-SNR-T	High-SNR-T	Low-SNR-T
0	0.0786	0.56362	0.86848	0.56345999	0.56378001	0.55552	0.56332001
5	0.0060	0.50562	0.65803999	0.50562	0.50564	0.50426	0.50558001
10	$3.8721 \times 10^{-6}$	0.50075999	0.50454	0.50075999	0.50075999	0.50075999	0.50075999
15	$9.1240 \times 10^{-16}$	0.50338	0.50338	0.50338	0.50338	0.50338	0.50338
20	$1.0442 \times 10^{-45}$	0.49835998	0.49835998	0.49835998	0.49835998	0.49835998	0.49835998
25	$7.3070 \times 10^{-140}$	0.49908	0.49908	0.49908	0.49908	0.49908	0.49908
30	0	0.49677998	0.49677998	0.49677998	0.49677998	0.49677998	0.49677998
35	0	0.50049999	0.50049999	0.50049999	0.50049999	0.50049999	0.50049999

TABLE 2: Numerical results II on bit error rate exhibited by optimal BPSK detector and ReLU FNN-based BPSK detectors.

SNR [in dB]	Optimal detector	ReLU FNN-based BPSK detector ( $K, H$ ) = (9, 9)			ReLU FNN-based BPSK detector ( $K, H$ ) = (9, 18)		
$\gamma_b$ [dB]	$\mathcal{Q}(\sqrt{2\gamma_b})$	All-SNR-T	High-SNR-T	Low-SNR-T	All-SNR-T	High-SNR-T	Low-SNR-T
0	0.0786	0.56356001	0.64416	0.56376001	0.56417999	0.55226001	0.565
5	0.0060	0.50562	0.52410001	0.50564	0.50567999	0.50376001	0.50588
10	$3.8721 \times 10^{-6}$	0.50075999	0.50080001	0.50075999	0.50075999	0.50075999	0.50075999
15	$9.1240 \times 10^{-16}$	0.50338	0.50338	0.50338	0.50338	0.50338	0.50338
20	$1.0442 \times 10^{-45}$	0.49835998	0.49835998	0.49835998	0.49835998	0.49835998	0.49835998
25	$7.3070 \times 10^{-140}$	0.49908	0.49908	0.49908	0.49908	0.49908	0.49908
30	0	0.49677998	0.49677998	0.49677998	0.49677998	0.49677998	0.49677998
35	0	0.50049999	0.50049999	0.50049999	0.50049999	0.50049999	0.50049999

TABLE 3: Numerical results III on bit error rate manifested by optimal BPSK detector and ReLU FNN-based BPSK detectors.

### 5.3 Results for ReLU FNNs

Using the (hyper)parameters of [70, Table VI], we produced the ReLU FNN-based BPSK detectors' testing and theory validation results that are presented in Sections 5.3.1 and 5.3.2, respectively.

#### 5.3.1 Testing Results

Tables 1-3 contrast the detection performance of the optimum BPSK detector and ReLU FNN-based BPSK detectors. Table 1 confirms that shallow ReLU FNNs with  $K = 3$  perform relatively well with Low-SNR-T better than with All-SNR-T or High-SNR-T for  $\gamma_b \in \{0, 5\}$  dB. Tables 2 and 3 validate that deep ReLU FNNs with  $K \in \{7, 9\}$  perform better with All-SNR-T than with Low-SNR-T or High-SNR-T for  $\gamma_b \in \{0, 5\}$  dB. Tables 1-3 substantiate that High-SNR-T produces the worst performance for  $\gamma_b \in \{0, 5\}$  dB; ReLU FNNs perform identically with All-SNR-T, High-SNR-T, and Low-SNR-T for  $\gamma_b > 5$  dB, irrespective of the networks' depth and width.

The minimum probability of bit error exhibited by a ReLU FNN-based BPSK detector irrespective of its width, depth, and training scheme is almost 0.5 as attested by Tables 1-3, which illustrate that a ReLU FNN-based BPSK detector trained with hinge loss and Adam fails to learn optimum BPSK detection. At high SNRs, a sampled BPSK signal is likely a large positive or negative number when bit 1 or bit 0 is transmitted over an AWGN channel, respectively. This detection problem is thus a simple inference problem that can be solved by using the decision threshold  $\tau_{th} = 0$ . Nonetheless, our best-trained deep (or shallow) ReLU FNNs fail at this common-sense inference task. This may be because FNNs (and deep networks in general) are poor at solving (common-sense) inference tasks [73] such as BPSK signal detection at high SNRs.

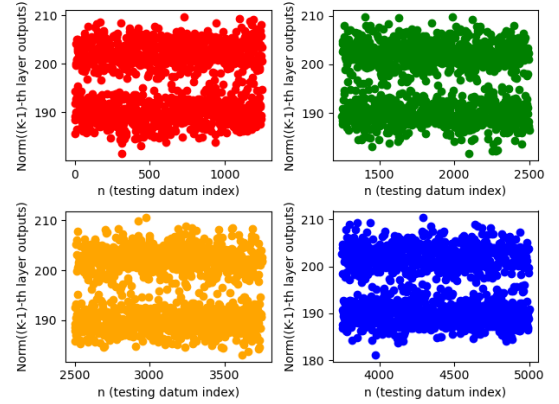


Fig. 1: A scatter plot of  $\|\mathbf{y}_{K-1,n}^{(T)}\|$  versus  $n$  under All-SNR-T,  $(K, H) = (8, 8)$ , and testing at 35 dB: the computed testing  $P_e$  at 35 dB is  $P_e = 0.50049999$ .

#### 5.3.2 Theory Validation Results

For shallow ReLU FNN-based BPSK detectors with  $(K, H) = (8, 8)$ , Figs. 1-3 show the scatter plots of  $\|\mathbf{y}_{K-1,n}^{(T)}\|$  versus  $n$  subject to All-SNR-T, High-SNR-T, and Low-SNR-T, respectively. These scatter plots do not exactly corroborate Theorem 1 since  $\|\mathbf{y}_{K-1,n}^{(T)}\|$  doesn't approach infinity or zero, though the testing  $P_e$  equals 0.5 in all cases.

As for deep ReLU FNN-based BPSK detectors with  $(K, H) = (16, 16)$ , Figs. 4-6 show the scatter plots of  $\|\mathbf{y}_{K-1,n}^{(T)}\|$  versus  $n$  subject to All-SNR-T, High-SNR-T, and Low-SNR-T, respectively. Fig. 5 corroborates Theorem 1 since the obtained  $P_e$  equals 0.5 and  $\|\mathbf{y}_{K-1,n}^{(T)}\|$  approaches either zero or a very large number. However, Theorem 1 is not validated by Figs. 4&6, which are among the results that cannot be interpreted by Theorem 1.



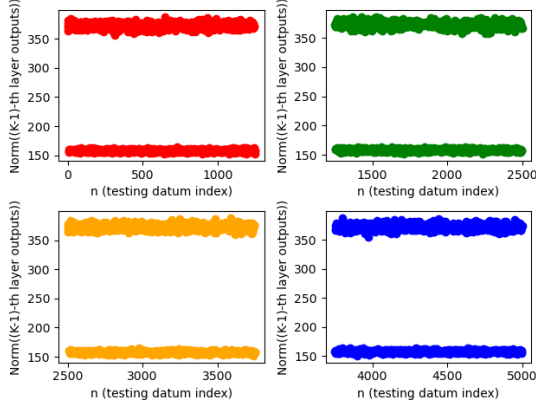


Fig. 2: A scatter plot of  $\|\mathbf{y}_{K-1,n}^{(T)}\|$  versus  $n$  under High-SNR-T,  $(K, H) = (8, 8)$ , and testing at 35 dB: the computed testing  $P_e$  at 35 dB is  $P_e = 0.50049999$ .

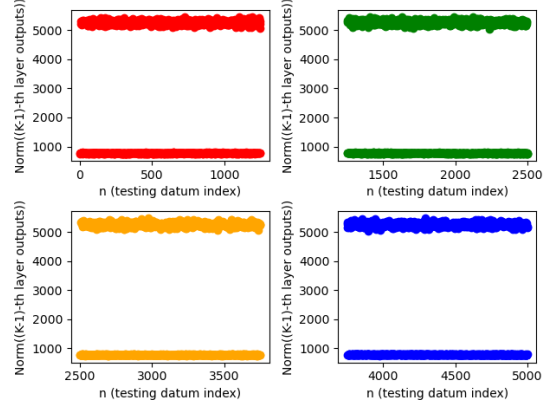


Fig. 5: A scatter plot of  $\|\mathbf{y}_{K-1,n}^{(T)}\|$  versus  $n$  under High-SNR-T,  $(K, H) = (16, 16)$ , and testing at 35 dB: the computed testing  $P_e$  at 35 dB is  $P_e = 0.50049999$ .

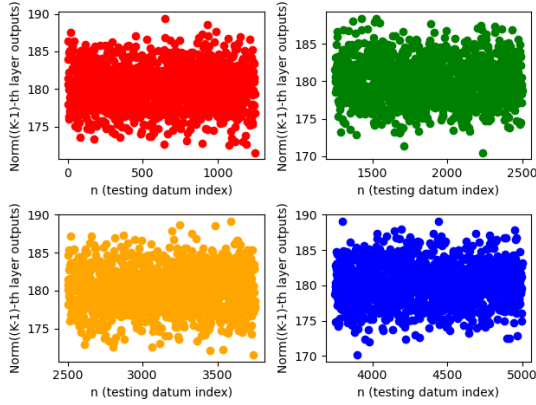


Fig. 3: A scatter plot of  $\|\mathbf{y}_{K-1,n}^{(T)}\|$  versus  $n$  under Low-SNR-T,  $(K, H) = (8, 8)$ , and testing at 35 dB: the computed testing  $P_e$  at 35 dB is  $P_e = 0.50049999$ .

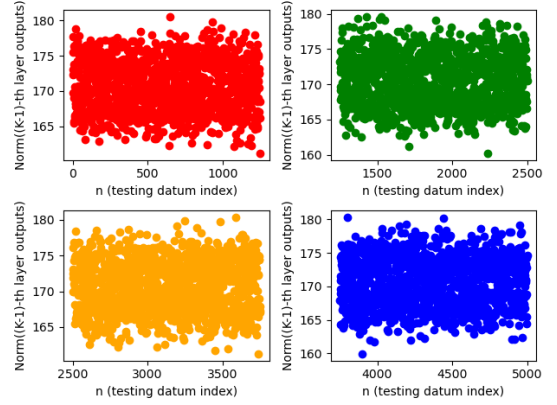


Fig. 6: A scatter plot of  $\|\mathbf{y}_{K-1,n}^{(T)}\|$  versus  $n$  under Low-SNR-T,  $(K, H) = (16, 16)$ , and testing at 35 dB: the computed testing  $P_e$  at 35 dB is  $P_e = 0.50049999$ .

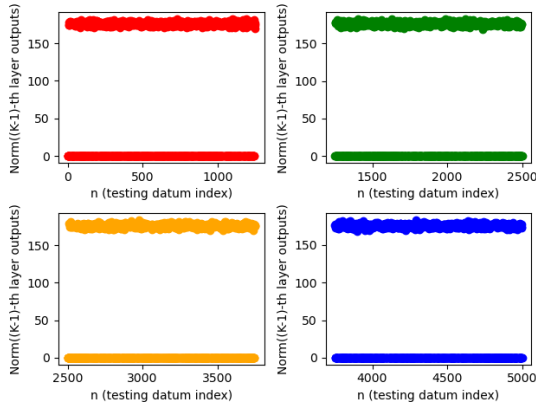


Fig. 4: A scatter plot of  $\|\mathbf{y}_{K-1,n}^{(T)}\|$  versus  $n$  under All-SNR-T,  $(K, H) = (16, 16)$ , and testing at 35 dB: the computed testing  $P_e$  at 35 dB is  $P_e = 1.0$ .

plots fail to validate Theorem 1 since the manifested  $P_e$  is always 1.0, affirming some testing results that cannot be interpreted using our theory.

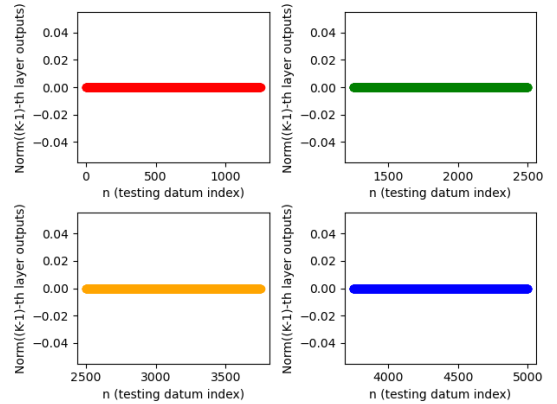


Fig. 7: A scatter plot of  $\|\mathbf{y}_{K-1,n}^{(T)}\|$  versus  $n$  under All-SNR-T,  $(K, H) = (20, 100)$ , and testing at 35 dB: the computed testing  $P_e$  at 35 dB is  $P_e = 1.0$ .

We now proceed to deep and wider ReLU FNN-based BPSK detectors. Figs. 7-9 show the scatter plots of  $\|\mathbf{y}_{K-1,n}^{(T)}\|$  versus  $n$  subject to All-SNR-T, High-SNR-T, and Low-SNR-T, respectively, for  $(K, H) = (20, 100)$ . These



SNR [in dB]	Optimal detector	FNN-based BPSK detector ( $K, H$ ) = (3, 3)			FNN-based BPSK detector ( $K, H$ ) = (3, 9)		
$\gamma_b$ [dB]	$\mathcal{Q}(\sqrt{2\gamma_b})$	All-SNR-T	High-SNR-T	Low-SNR-T	All-SNR-T	High-SNR-T	Low-SNR-T
0	0.0786	0.54196	0.60334	0.54232001	0.54198	0.57132	0.54192001
5	0.0060	0.50231999	0.51339999	0.50235999	0.50231999	0.50687999	0.50229999
10	$3.8721 \times 10^{-6}$	0.50075999	0.50075999	0.50075999	0.50075999	0.50075999	0.50075999
15	$9.1240 \times 10^{-16}$	0.50338	0.50338	0.50338	0.50338	0.50338	0.50338
20	$1.0442 \times 10^{-45}$	0.49835998	0.49835998	0.49835998	0.49835998	0.49835998	0.49835998
25	$7.3070 \times 10^{-140}$	0.49908	0.49908	0.49908	0.49908	0.49908	0.49908
30	0	0.49677998	0.49677998	0.49677998	0.49677998	0.49677998	0.49677998
35	0	0.50049999	0.50049999	0.50049999	0.50049999	0.50049999	0.50049999

TABLE 4: Numerical results I on bit error rate manifested by optimal BPSK detector and BPSK detectors based on FNNs with ReLU and Tanh activation.

SNR [in dB]	Optimal detector	FNN-based BPSK detector ( $K, H$ ) = (4, 8)			FNN-based BPSK detector ( $K, H$ ) = (7, 7)		
$\gamma_b$ [dB]	$\mathcal{Q}(\sqrt{2\gamma_b})$	All-SNR-T	High-SNR-T	Low-SNR-T	All-SNR-T	High-SNR-T	Low-SNR-T
0	0.0786	0.54194	0.58012	0.54179999	0.54192001	0.60139999	0.54192001
5	0.0060	0.50229999	0.50854	0.50226	0.50229999	0.51298001	0.50229999
10	$3.8721 \times 10^{-6}$	0.50075999	0.50075999	0.50075999	0.50075999	0.50075999	0.50075999
15	$9.1240 \times 10^{-16}$	0.50338	0.50338	0.50338	0.50338	0.50338	0.50338
20	$1.0442 \times 10^{-45}$	0.49835998	0.49835998	0.49835998	0.49835998	0.49835998	0.49835998
25	$7.3070 \times 10^{-140}$	0.49908	0.49908	0.49908	0.49908	0.49908	0.49908
30	0	0.49677998	0.49677998	0.49677998	0.49677998	0.49677998	0.49677998
35	0	0.50049999	0.50049999	0.50049999	0.50049999	0.50049999	0.50049999

TABLE 5: Numerical results II on bit error rate manifested by optimal BPSK detector and BPSK detectors based on FNNs with ReLU and Tanh activation.

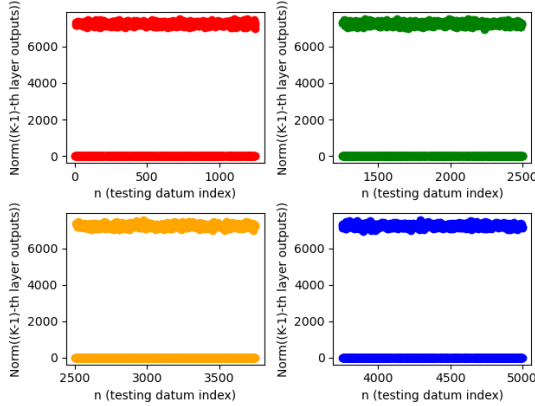


Fig. 8: A scatter plot of  $\|\mathbf{y}_{K-1,n}^{(T)}\|$  versus  $n$  under High-SNR-T, ( $K, H$ ) = (20, 100), and testing at 35 dB: the computed testing  $P_e$  at 35 dB is  $P_e = 1.0$ .

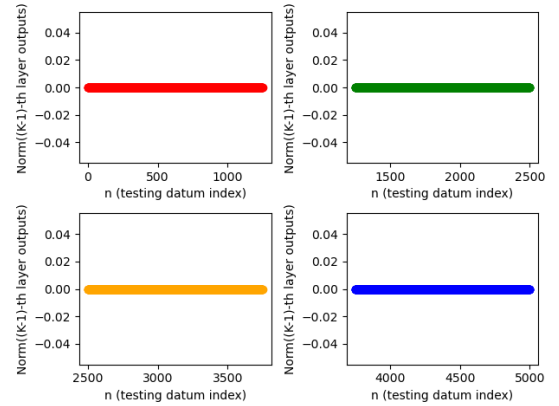


Fig. 9: A scatter plot of  $\|\mathbf{y}_{K-1,n}^{(T)}\|$  versus  $n$  under Low-SNR-T, ( $K, H$ ) = (20, 100), and testing at 35 dB: the computed testing  $P_e$  at 35 dB is  $P_e = 1.0$ .

## 5.4 Results for FNNs with ReLU and Tanh Activation

Employing the (hyper)parameters of [70, Table VII], we generated the testing and theory validation results – presented in Sections 5.4.1 and 5.4.2, respectively – for BPSK detectors based on FNNs with ReLU and Tanh activation.

### 5.4.1 Testing Results

The numerical results for BPSK detectors based on FNNs with ReLU and Tanh activation are provided in Tables 4 and 5. As seen in those tables, BPSK detectors based on FNNs – with ReLU and Tanh activation – trained with hinge loss and Adam fail to learn optimum BPSK detection for any SNR.

### 5.4.2 Theory Validation Results

As to the BPSK detectors based on shallow FNNs with ReLU and Tanh activation, Figs. 10-12 show the scatter plots of  $\|\mathbf{y}_{K-1,n}^{(T)}\|$  versus  $n$  subject to All-SNR-T, High-SNR-T, and Low-SNR-T, respectively, for ( $K, H$ ) = (8, 8). Figs. 10&12 validate Theorem 2 since the exhibited  $\hat{P}_e$  equals 0.5 and  $\|\mathbf{y}_{K-1,n}^{(T)}\|$  tends to zero or infinity. However, Theorem 2 is not verified by Fig. 11, which is among the results that cannot be interpreted by our developed theory.

As for the BPSK detectors based on deep and wider FNNs with ReLU and Tanh activation, Figs. 13-15 show the scatter plots of  $\|\mathbf{y}_{K-1,n}^{(T)}\|$  versus  $n$  subject to All-SNR-T, High-SNR-T, and Low-SNR-T, respectively, for ( $K, H$ ) =

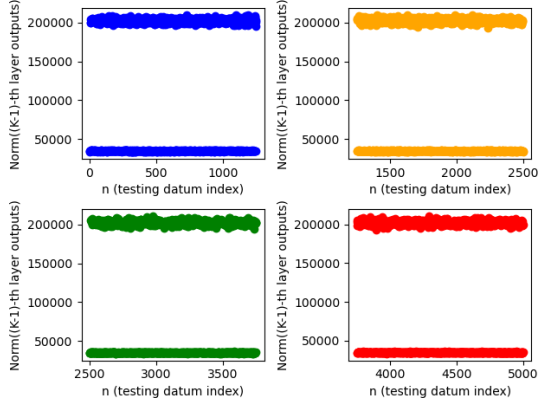


Fig. 10: A scatter plot of  $\|\tilde{\mathbf{y}}_{K-1,n}^{(T)}\|$  versus  $n$  under All-SNR-T,  $(K, H) = (8, 8)$ , and testing at 35 dB: the computed testing  $\tilde{P}_e$  at 35 dB is  $\tilde{P}_e = 0.50049999$ .

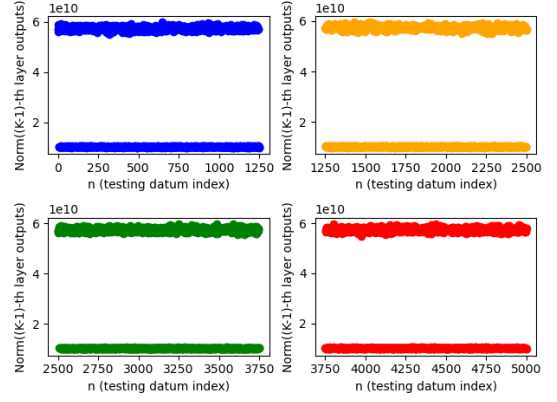


Fig. 13: A scatter plot of  $\|\tilde{\mathbf{y}}_{K-1,n}^{(T)}\|$  versus  $n$  under All-SNR-T,  $(K, H) = (20, 100)$ , and testing at 35 dB: the computed testing  $\tilde{P}_e$  at 35 dB is  $\tilde{P}_e = 0.50049999$ .

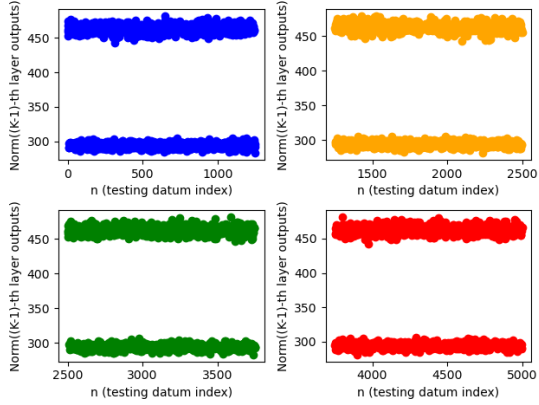


Fig. 11: A scatter plot of  $\|\tilde{\mathbf{y}}_{K-1,n}^{(T)}\|$  versus  $n$  under High-SNR-T,  $(K, H) = (8, 8)$ , and testing at 35 dB: the computed testing  $\tilde{P}_e$  at 35 dB is  $\tilde{P}_e = 0.50049999$ .

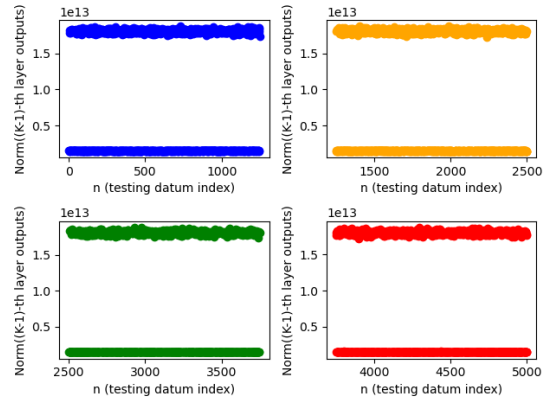


Fig. 14: A scatter plot of  $\|\tilde{\mathbf{y}}_{K-1,n}^{(T)}\|$  versus  $n$  under High-SNR-T,  $(K, H) = (20, 100)$ , and testing at 35 dB: the computed testing  $\tilde{P}_e$  at 35 dB is  $\tilde{P}_e = 1.0$ .

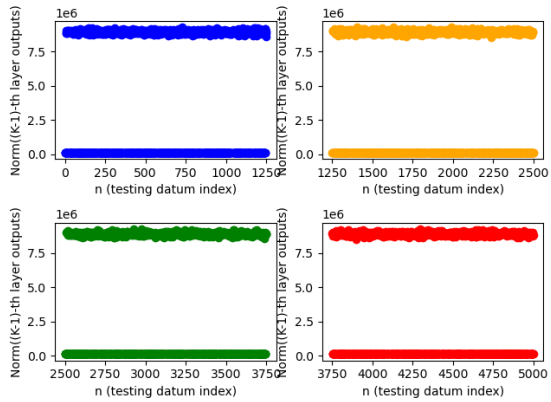


Fig. 12: A scatter plot of  $\|\tilde{\mathbf{y}}_{K-1,n}^{(T)}\|$  versus  $n$  under Low-SNR-T,  $(K, H) = (8, 8)$ , and testing at 35 dB: the computed testing  $\tilde{P}_e$  at 35 dB is  $\tilde{P}_e = 0.50049999$ .

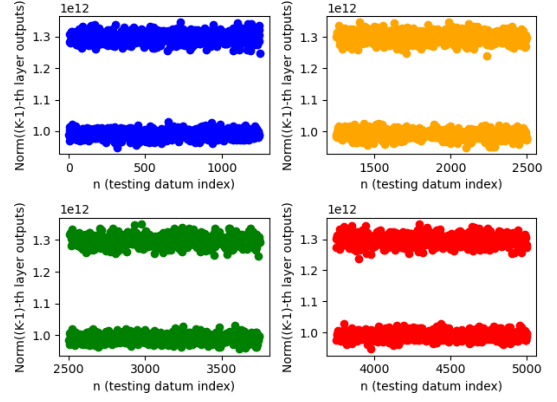


Fig. 15: A scatter plot of  $\|\tilde{\mathbf{y}}_{K-1,n}^{(T)}\|$  versus  $n$  under Low-SNR-T,  $(K, H) = (20, 100)$ , and testing at 35 dB: the computed testing  $\tilde{P}_e$  at 35 dB is  $\tilde{P}_e = 0.50049999$ .

$(20, 100)$ . Figs. 13&15 validate Theorem 2 because the manifested  $\tilde{P}_e$  equals 0.5 and  $\|\tilde{\mathbf{y}}_{K-1,n}^{(T)}\|$  tends to zero or infinity. Nevertheless, Theorem 2 is not validated by Fig. 14, which is among the testing results uninterpretable by our theory.

## 6 CONCLUSIONS AND RESEARCH OUTLOOK

Despite DL's broad impacts and successes, a comprehensive insight on why and how DL is empirically successful in astronomically many AI/ML problems remains funda-

mentally elusive. In this vein, no fundamental work has managed yet to quantify the testing performance limits of DL-based classifiers trained with cross-entropy loss or hinge loss. To overcome this limitation in part, we developed a theory for the asymptotic testing performance limits of deep ReLU FNNs and deep FNNs with ReLU and Tanh activation. Our theory is an intuitive one that interprets some results of our extensive computer experiments, especially as the corresponding FNNs get deeper and wider.

Important research outlook is developing a fundamental theory on the non-asymptotic performance limits of binary classifiers based on *i)* deep ReLU FNNs and *ii)* deep FNNs with ReLU and Tanh activation. What is also important is determining the fundamental testing performance limits of DL-based multi-level classifiers trained using cross-entropy loss, which undoubtedly entails more complex decision regions/boundaries.

## ACKNOWLEDGMENTS

T. M. Getu acknowledges Prof. Ali H. Sayed (EPFL, Switzerland) for fruitful discussions and criticisms; the U.S. Department of Commerce and its agency NIST for a computational support and a prior funding support.

## REFERENCES

- [1] Y. Lecun, Y. Bengio, and G. Hinton, "Deep learning," *Nature*, vol. 521, pp. 436–444, May 2015.
- [2] A. W. Senior *et al.*, "Improved protein structure prediction using potentials from deep learning," *Nature*, vol. 577, pp. 706–710, 2020.
- [3] J. Ma, R. P. Sheridan, A. Liaw, G. E. Dahl, and V. Svetnik, "Deep neural nets as a method for quantitative structure-activity relationships," *J. Chem. Inf. Model.*, vol. 55, pp. 263–74, 2015.
- [4] V. Mnih *et al.*, "Human-level control through deep reinforcement learning," *Nature*, vol. 518, no. 7540, pp. 529–533, 2015.
- [5] David Silver *et al.*, "Mastering the game of Go with deep neural networks and tree search," *Nature*, vol. 529, pp. 484–489, 2016.
- [6] T. Young, D. Hazarika, S. Poria, and E. Cambria, "Recent trends in deep learning based natural language processing," *IEEE Comput. Intell. Mag.*, vol. 13, no. 3, pp. 55–75, 2018.
- [7] G. Hinton, L. Deng, D. Yu, G. E. Dahl, A.-r. Mohamed, N. Jaitly, A. Senior, V. Vanhoucke, P. Nguyen, T. N. Sainath, and B. Kingsbury, "Deep neural networks for acoustic modeling in speech recognition: The shared views of four research groups," *IEEE Signal Process. Mag.*, vol. 29, no. 6, pp. 82–97, 2012.
- [8] C. Zhang, P. Patras, and H. Haddadi, "Deep learning in mobile and wireless networking: A survey," *IEEE Commun. Surv. Tutor.*, vol. 21, no. 3, pp. 2224–2287, 3rd Quart. 2019.
- [9] Q. Mao, F. Hu, and Q. Hao, "Deep learning for intelligent wireless networks: A comprehensive survey," *IEEE Commun. Surv. Tutor.*, vol. 20, no. 4, pp. 2595–2621, 4th Quart. 2018.
- [10] T. H. Trinh, Y. Wu, Q. V. Le, Quoc, H. He, and T. Luong, "Solving olympiad geometry without human demonstrations," *Nature*, vol. 625, pp. 476–482, Jan. 2024.
- [11] J. Han, A. Jentzen, and W. E., "Solving high-dimensional partial differential equations using deep learning," *Proc. Natl. Acad. Sci. U.S.A.*, vol. 115, no. 34, pp. 8505–8510, 2018.
- [12] A. Esteva, B. Kuprel, R. A. Novoa, J. M. Ko, S. M. Swetter, H. M. Blau, and S. Thrun, "Dermatologist-level classification of skin cancer with deep neural networks," *Nature*, vol. 542, pp. 115–118, 2017.
- [13] J. De Fauw *et al.*, "Clinically applicable deep learning for diagnosis and referral in retinal disease," *Nat. Med.*, vol. 24, pp. 1342–1350, 2018.
- [14] A. Radhakrishnan, M. Belkin, and C. Uhler, "Overparameterized neural networks implement associative memory," *Proc. Natl. Acad. Sci. U.S.A.*, vol. 117, no. 44, pp. 27 162–27 170, 2020.
- [15] A. M. Saxe, J. L. McClelland, and S. Ganguli, "A mathematical theory of semantic development in deep neural networks," *Proc. Natl. Acad. Sci. U.S.A.*, vol. 116, no. 23, pp. 11 537–11 546, 2019.
- [16] G. Carleo and M. Troyer, "Solving the quantum many-body problem with artificial neural networks," *Science*, vol. 355, no. 6325, pp. 602–606, 2017.
- [17] Y. Levine, O. Sharir, N. Cohen, and A. Shashua, "Quantum entanglement in deep learning architectures," *Phys. Rev. Lett.*, vol. 122, p. 065301, Feb. 2019.
- [18] P. Baldi, P. Sadowski, and D. Whiteson, "Searching for exotic particles in high-energy physics with deep learning," *Nat. Commun.*, vol. 5, Jul. 2014.
- [19] Y. Bengio, A. Courville, and P. Vincent, "Representation learning: A review and new perspectives," *IEEE Trans. Pattern Anal. Mach. Intell.*, vol. 35, no. 8, pp. 1798–1828, Aug. 2013.
- [20] D. Castelvecchi, "The Black Box of AI," *Nature*, vol. 538, pp. 20–23, Oct. 2016.
- [21] T. Poggio, A. Banburski, and Q. Liao, "Theoretical issues in deep networks," *Proc. Natl. Acad. Sci. U.S.A.*, Jun. 2020.
- [22] J. Berner, P. Grohs, G. Kutyniok, and P. Petersen, "The modern mathematics of deep learning," 2021. [Online]. Available: <https://arxiv.org/pdf/2105.04026.pdf>
- [23] P. L. Bartlett, A. Montanari, and A. Rakhlin, "Deep learning: a statistical viewpoint," *Acta Numer.*, vol. 30, pp. 87 – 201, 2021.
- [24] H. N. Mhaskar, "Neural networks for optimal approximation of smooth and analytic functions," *Neural Comput.*, vol. 8, pp. 164–177, 1996.
- [25] A. Pinkus, "Approximation theory of the MLP model in neural networks," *Acta Numerica*, vol. 8, pp. 143–195, 1999.
- [26] D. Rolnick and M. Tegmark, "The power of deeper networks for expressing natural functions," in *Proc. ICLR*, 2018.
- [27] B. Poole, S. Lahiri, M. Raghu, J. Sohl-Dickstein, and S. Ganguli, "Exponential expressivity in deep neural networks through transient chaos," in *Proc. NIPS*, 2016, pp. 3368–3376.
- [28] H. W. Lin, M. Tegmark, and D. Rolnick, "Why does deep and cheap learning work so well?" *J. Stat. Phys.*, vol. 168, no. 6, pp. 1223–1247, Jul. 2017.
- [29] R. Eldan and O. Shamir, "The power of depth for feedforward neural networks," in *Proc. COLT*, 2016, pp. 907–940.
- [30] H. Mhaskar and T. Poggio, "Deep vs. shallow networks : An approximation theory perspective." [Online]. Available: <https://arxiv.org/pdf/1608.03287.pdf>
- [31] T. Poggio, H. Mhaskar, L. Rosasco, B. Miranda, and Q. Liao, "Why and when can deep-but not shallow-networks avoid the curse of dimensionality: A review," *Int. J. Autom. Comput.*, vol. 14, pp. 503–519, Dec. 2017.
- [32] Z. Lu, H. Pu, F. Wang, Z. Hu, and L. Wang, "The expressive power of neural networks: A view from the width," in *Proc. NIPS*, 2017, pp. 6232–6240.
- [33] F.-L. Fan and G. Wang, "Duality of width and depth of neural networks." [Online]. Available: <https://arxiv.org/pdf/2002.02515.pdf>
- [34] F. Fan, D. Wang, H. Guo, Q. Zhu, P. Yan, G. Wang, and H. Yu, "Slim, sparse, and shortcut networks," 2018. [Online]. Available: <https://arxiv.org/pdf/1811.09003v2.pdf>
- [35] I. Daubechies, R. DeVore, S. Foucart, B. Hanin, and G. Petrova, "Nonlinear approximation and (deep) ReLU networks," 2019.
- [36] A. R. Barron and J. M. Klusowski, "Approximation and estimation for high-dimensional deep learning networks," 2018. [Online]. Available: <https://arxiv.org/pdf/1809.03090.pdf>
- [37] T. M. Getu, "Error bounds for a matrix-vector product approximation with deep ReLU neural networks," 2021. [Online]. Available: <https://arxiv.org/pdf/2111.12963.pdf>
- [38] B. Hanin, "Universal function approximation by deep neural nets with bounded width and ReLU activations," *Mathematics*, vol. 7, 2019.
- [39] D. Elbrächter, D. Perekrestenko, P. Grohs, and H. Bölcskei, "Deep neural network approximation theory," *IEEE Trans. Inf. Theory*, vol. 67, no. 5, pp. 2581–2623, 2021.
- [40] H. Bölcskei, P. Grohs, G. Kutyniok, and P. Petersen, "Optimal approximation with sparsely connected deep neural networks," *SIAM J. Math. Data Sci.*, vol. 1, no. 1, pp. 8–45, 2019.
- [41] P. Petersen and F. Voigtlaender, "Optimal approximation of piecewise smooth functions using deep ReLU neural networks," *Neural Netw.*, vol. 108, pp. 296–330, Dec. 2018.
- [42] M. Geiger, L. Petrini, and M. Wyart, "Landscape and training regimes in deep learning," *Phys. Rep.*, vol. 924, pp. 1–18, 2021.
- [43] R. Sun, D. Li, S. Liang, T. Ding, and R. Srikant, "The global landscape of neural networks: An overview," *IEEE Signal Process. Mag.*, vol. 37, no. 5, pp. 95–108, 2020.

- [44] C. Baldassi, C. Borgs, J. T. Chayes, A. Ingrosso, C. Lucibello, L. Saglietti, and R. Zecchina, "Unreasonable effectiveness of learning neural networks: From accessible states and robust ensembles to basic algorithmic schemes," *Proc. Natl. Acad. Sci. U.S.A.*, vol. 113, no. 48, pp. E7655–E7662, 2016.
- [45] C. Baldassi, F. Pittorino, and R. Zecchina, "Shaping the learning landscape in neural networks around wide flat minima," *Proc. Natl. Acad. Sci. U.S.A.*, vol. 117, no. 1, pp. 161–170, 2020.
- [46] M. Belkin, D. J. Hsu, S. Ma, and S. Mandal, "Reconciling modern machine-learning practice and the classical bias–variance trade-off," *Proc. Natl. Acad. Sci. U.S.A.*, vol. 116, pp. 15 849–15 854, 2019.
- [47] R. Livni, S. Shalev-Shwartz, and O. Shamir, "On the computational efficiency of training neural networks," in *Proc. NIPS*, vol. 27, 2014.
- [48] A. Jacot, F. Gabriel, and C. Hongler, "Neural tangent kernel: Convergence and generalization in neural networks," in *Proc. NIPS*, 2018, pp. 8571–8580.
- [49] L. Chizat, E. Oyallon, and F. Bach, "On lazy training in differentiable programming," Jan. 2020. [Online]. Available: <https://arxiv.org/pdf/1812.07956.pdf>
- [50] Z. Allen-Zhu, Y. Li, and Z. Song, "A convergence theory for deep learning via over-parameterization," 2018. [Online]. Available: <https://arxiv.org/pdf/1811.03962.pdf>
- [51] D. Zou, Y. Cao, D. Zhou, and Q. Gu, "Stochastic gradient descent optimizes over-parameterized deep ReLU networks," 2018. [Online]. Available: <https://arxiv.org/pdf/1811.08888.pdf>
- [52] H. Zhang, D. Yu, M. Yi, W. Chen, and T.-Y. Liu, "Convergence theory of learning over-parameterized ResNet: A full characterization," 2019. [Online]. Available: <https://arxiv.org/pdf/1903.07120v2.pdf>
- [53] M. Soltanolkotabi, A. Javanmard, and J. D. Lee, "Theoretical insights into the optimization landscape of over-parameterized shallow neural networks," *IEEE Trans. Inf. Theory*, vol. 65, no. 2, pp. 742–769, 2019.
- [54] Z. Chen, Y. Cao, D. Zou, and Q. Gu, "How much over-parameterization is sufficient to learn deep ReLU networks?" 2020. [Online]. Available: <https://arxiv.org/pdf/1911.12360.pdf>
- [55] Z. Allen-Zhu, Y. Li, and Y. Liang, "Learning and generalization in overparameterized neural networks, going beyond two layers," 2020. [Online]. Available: <https://arxiv.org/pdf/1811.04918.pdf>
- [56] Y. Cao and Q. Gu, "Generalization error bounds of gradient descent for learning over-parameterized deep ReLU networks," 2019. [Online]. Available: <https://arxiv.org/pdf/1902.01384.pdf>
- [57] C. Zhang, S. Bengio, M. Hardt, B. Recht, and O. Vinyals, "Understanding deep learning requires rethinking generalization," 2017.
- [58] B. Adlam and J. Pennington, "The neural tangent kernel in high dimensions: Triple descent and a multi-scale theory of generalization. arxiv [preprint]. <https://arxiv.org/pdf/2008.06786.pdf> (accessed Dec. 2021)." 2020.
- [59] S. Mei, A. Montanari, and P.-M. Nguyen, "A mean field view of the landscape of two-layer neural networks," *Proc. Natl. Acad. Sci. U.S.A.*, vol. 115, no. 33, pp. E7665–E7671, 2018.
- [60] P.-M. Nguyen and H. T. Pham, "A rigorous framework for the mean field limit of multilayer neural networks. arxiv [preprint]. <https://arxiv.org/pdf/2001.11443.pdf> (accessed Jul. 2021)." 2021.
- [61] V. Pappas, X. Y. Han, and D. L. Donoho, "Prevalence of neural collapse during the terminal phase of deep learning training," *Proc. Natl. Acad. Sci. U.S.A.*, vol. 117, no. 40, pp. 24 652–24 663, 2020.
- [62] C. Fang, H. He, Q. Long, and W. J. Su, "Exploring deep neural networks via layer-peeled model: Minority collapse in imbalanced training," *Proc. Natl. Acad. Sci. U.S.A.*, vol. 118, no. 43, 2021.
- [63] S. Haykin, *Neural Networks and Learning Machines*, 3rd ed. Upper Saddle River, NJ, USA: Pearson, 2009.
- [64] S. Shalev-Shwartz and S. Ben-David, *Understanding Machine Learning: From Theory to Algorithms*. New York, NY, USA: Cambridge Univ. Press, 2014.
- [65] W. E. C. Ma, S. Wojtowytsch, and L. Wu, "Towards a mathematical understanding of neural network-based machine learning: what we know and what we don't," 2020. [Online]. Available: <https://arxiv.org/pdf/2009.10713.pdf>
- [66] M. J. Wainwright, *High-Dimensional Statistics: A Non-Asymptotic Viewpoint*. Cambridge Univ. Press, 2019.
- [67] T. M. Getu, N. T. Golmie, and D. W. Griffith, "Blind estimation of a doubly selective OFDM channel: A deep learning algorithm and theory," 2022. [Online]. Available: <https://arxiv.org/pdf/2206.07483.pdf>
- [68] T. M. Getu, W. Saad, G. Kaddoum, and M. Bennis, "Performance limits of a deep learning-enabled text semantic communication under interference," *IEEE Trans. Wirel. Commun.*, vol. 23, no. 8, pp. 10 213–10 228, Aug. 2024.
- [69] I. Gühring, G. Kutyniok, and P. Petersen, "Error bounds for approximations with deep ReLU neural networks in  $W^{s,p}$  norms," *Anal. Appl.*, vol. 18, Aug. 2019.
- [70] T. M. Getu and G. Kaddoum, "Fundamental limits of deep learning-based binary classifiers trained with hinge loss," 2023. [Online]. Available: <https://arxiv.org/pdf/2309.06774v1.pdf>
- [71] G. Wang, G. B. Giannakis, and J. Chen, "Learning ReLU networks on linearly separable data: Algorithm, optimality, and generalization," *IEEE Trans. Signal Process.*, vol. 67, pp. 2357–2370, 2019.
- [72] F. Chollet, *Deep Learning with Python*. Shelter Island, NY, USA: Manning, 2018.
- [73] G. Marcus, "Deep learning: A critical appraisal," 2018. [Online]. Available: <https://arxiv.org/abs/1801.00631>



**Tilahun M. Getu** (M'19) earned the Ph.D. degree (with highest honor) in electrical engineering from the École de Technologie Supérieure (ÉTS), Montreal, QC, Canada in 2019. He is currently a Post-doctoral Fellow with the ÉTS. His transdisciplinary fundamental research interests span the numerous fields of classical and quantum Science, Technology, Engineering, and Mathematics (STEM) at the nexus of communications, signal processing, and networking (all types); intelligence (both artificial and natural); robotics; computing; security; optimization; high-dimensional statistics; and high-dimensional causal inference.

Dr. Getu has received several awards, including the 2019 ÉTS Board of Directors Doctoral Excellence Award in recognition of his Ph.D. dissertation selected as the 2019 ÉTS all-university best Ph.D. dissertation.



**Georges Kaddoum** (M'11–SM'20) is a professor and Tier 2 Canada Research Chair with the École de Technologie Supérieure (ÉTS), Université du Québec, Montréal, Canada. He is also a Faculty Fellow in the Cyber Security Systems and Applied AI Research Center at Lebanese American University. His recent research activities cover 5G/6G networks, tactical communications, resource allocations, and security. Dr. Kaddoum has received many prestigious national and international awards in recognition of his

outstanding research outcomes. Currently, Prof. Kaddoum serves as an Area Editor for the IEEE Transactions on Machine Learning in Communications and Networking and an Associate Editor for IEEE Transactions on Information Forensics and Security, and IEEE Transactions on Communications.



**Mehdi Bennis** (F'20) is a full tenured Professor at the Centre for Wireless Communications, University of Oulu, Finland and head of the Intelligent COnnectivity and Networks/Systems Group (ICON). His main research interests are in radio resource management, game theory and distributed AI in 5G/6G networks. He has published more than 200 research papers in international conferences, journals and book chapters. He has been the recipient of several prestigious awards. Dr. Bennis is an editor of IEEE TCOM

and Specialty Chief Editor for Data Science for Communications in the Frontiers in Communications and Networks journal.

# Supplementary Material

Tilahun M. Getu, *Member, IEEE*, Georges Kaddoum, *Senior Member, IEEE*,  
and Mehdi Bennis, *Fellow, IEEE*

## Abstract

As a supplementary material to our *IEEE PAMI* paper entitled “Fundamental Limits of Deep Learning-Based Binary Classifiers Trained with Hinge Loss”, this paper documents the proofs of our theorems on the fundamental asymptotic performance limits of binary classifiers based on rectified linear unit (ReLU) feedforward neural networks (FNNs) and FNNs with ReLU and Tanh activation.

## Index Terms

Theorem proof.



## 1 NOTATION

Scalars, vectors, and matrices are represented by italic, bold lowercase, and bold uppercase letters, respectively. Uppercase italic letters denote random variables. Uppercase calligraphic letters denote events and hypotheses.  $\mathbb{R}$ ,  $\mathbb{R}_+$ ,  $\mathbb{R}^n$ ,  $\mathbb{R}^{m \times n}$ , and  $\mathbb{R}_+^{m \times n}$  denote the sets of real numbers, positive real numbers,  $n$ -dimensional real vectors,  $m \times n$  real matrices, and  $m \times n$  positive real matrices, respectively.  $\sim$ ,  $:=$ ,  $\mathbf{0}$ ,  $\exp(\cdot)$ , and  $\mathbb{P}(\cdot)$  stand for distributed as, equal by definition, a zero vector/matrix whose dimension will be clear in context, exponential function, and probability, respectively.  $\text{diag}(\cdot)$ ,  $\mathcal{N}(\mu, \sigma^2)$ ,  $(\cdot)^\top$ , and  $\mathbb{I}\{\cdot\}$  stand for a diagonal matrix, Gaussian distribution with mean  $\mu$  and variance  $\sigma^2$ , transpose, and a (component-wise) indicator function that returns 1 if the argument is true and 0 otherwise, respectively.  $\|\cdot\|$ ,  $\delta(\cdot)$ ,  $\ln(\cdot)$ ,  $\max(\cdot, \dots, \cdot)$ , and  $\min(\cdot, \dots, \cdot)$  stand for a vector norm, the Dirac delta function, the natural logarithm, maximum, and minimum, respectively. For  $\mathbf{a} \in \mathbb{R}^n$ ,  $(\mathbf{a})_i$  denotes the  $i$ -th entry of  $\mathbf{a}$ .  $Q(\cdot)$  stands for the  $Q$ -function defined for  $x \in \mathbb{R}$  as [1]

$$Q(x) := \frac{1}{\sqrt{2\pi}} \int_x^\infty \exp(-t^2/2) dt. \quad (1)$$

## 2 PROOF OF THEOREM 1

**Theorem 1.** Consider a (deep) ReLU FNN  $\Phi^{(T)} := [[\mathbf{w}_1^{(T)}, \mathbf{0}], [\mathbf{W}_2^{(T)}, \mathbf{0}], \dots, [\mathbf{W}_{K-1}^{(T)}, \mathbf{0}], [\mathbf{w}_K^{(T)}, \mathbf{0}]]$  – such that  $\mathbf{w}_K^{(T)} \in \mathbb{R}^{1 \times 2H}$ ,  $\mathbf{W}_{K-k}^{(T)} \in \mathbb{R}^{2H \times 2H}$  for all  $k \in [K-2]$ , and  $\mathbf{w}_1^{(T)} \in \mathbb{R}^{2H}$  – trained over  $\mathcal{D} := \{(x_n, y_n)\}_{n=1}^N$  using hinge loss and SGD, SGD with momentum, RMSProp, or Adam after being

T. M. Getu is with the Electrical Engineering Department, École de Technologie Supérieure (ETS), Montréal, QC H3C 1K3, Canada (e-mail: tilahun-melkamu.getu.1@ens.etsmtl.ca).

G. Kaddoum is with the Electrical Engineering Department, École de Technologie Supérieure (ETS), Montréal, QC H3C 1K3, Canada (e-mail: georges.kaddoum@etsmtl.ca).

M. Bennis is with the Centre for Wireless Communications, University of Oulu, 90570 Oulu, Finland (e-mail: mehdi.bennis@oulu.fi).

initialized by a Gaussian initializer such as LeCun normal or He normal, and to be tested over  $\mathcal{T} := \{(x_n, y_n)\}_{n=N+1}^{N+\tilde{N}}$ , given  $H, K, N, \tilde{N}, T \in \mathbb{N}$ . For  $N, \tilde{N}, T, K \geq 2$ , and  $H < \infty$ :

$$\lim_{\|\mathbf{y}_{K-1,n}^{(T)}\| \rightarrow \infty} P_e \leq 1/2 \quad (2a)$$

$$\lim_{(\|\mathbf{y}_{K-1,n}^{(T)}\|_{\mathcal{H}_{-1}}, \|\mathbf{y}_{K-1,n}^{(T)}\|_{\mathcal{H}_1}) \rightarrow (0, \infty)} P_e \leq 1/2, \quad (2b)$$

where (2a) and (2b) are valid for all  $n \in \{N+1, \dots, N+\tilde{N}\}$ .

### Proof of Theorem 1

For a trained deep ReLU FNN  $\Phi^{(T)}$ , it follows through [2, eq. (28)] that

$$\Phi^{(T)}(x_n) = \mathbf{w}_K^{(T)} \mathbf{y}_{K-1,n}^{(T)} = \sum_{q=1}^{2H} (\mathbf{w}_K^{(T)})_q (\mathbf{y}_{K-1,n}^{(T)})_q \in \mathbb{R}, \quad (3)$$

where  $\mathbf{y}_{K-1,n}^{(T)} = \left( \prod_{k=1}^{K-2} \Sigma_{K-k,n}^{(T)} \mathbf{W}_{K-k}^{(T)} \right) \Sigma_{1,n}^{(T)} \mathbf{w}_1^{(T)} x_n \in \mathbb{R}_+^{2H}$  – as defined via [2, eq. (29)] – for  $\Sigma_{1,n}^{(T)} = \text{diag}(\mathbb{I}\{\mathbf{w}_1^{(T)} x_n \geq 0\}) \in \{0, 1\}^{2H \times 2H}$  and  $\Sigma_{k,n}^{(T)} = \text{diag}(\mathbb{I}\{\mathbf{W}_k^{(T)} (\prod_{l=1}^{k-2} \Sigma_{K-l,n}^{(T)} \mathbf{W}_{K-l}^{(T)}) \Sigma_{1,n}^{(T)} \mathbf{w}_1^{(T)} x_n \geq 0\}) \in \{0, 1\}^{2H \times 2H}$ . The  $K$ -th FNN layer's weights at convergence  $\mathbf{w}_K^{(T)} \in \mathbb{R}^{1 \times 2H}$  is given through [2, (34c)]  $\forall q \in [2H]$  as

$$(\mathbf{w}_K^{(T)})_q = (\mathbf{w}_K)_q + \sum_{t=0}^{T-1} (\Delta \mathbf{w}_K^{(t)})_q, \quad (4)$$

where  $(\mathbf{w}_K)_q := (\mathbf{w}_K^{(0)})_q$  is initialized with a Gaussian initializer such as LeCun normal or He normal and hence  $(\mathbf{w}_K)_q \sim \mathcal{N}(0, \alpha/2H)$  for  $\alpha \in \{1, 2\}$  ( $\alpha = 1$  for LeCun normal and  $\alpha = 2$  for He normal); and  $\Delta \mathbf{w}_K^{(t)}$  is the weight correction during the  $t$ -th iteration of SGD, SGD with momentum, RMSProp, or Adam.

Substituting (4) into the RHS of (3) gives (5),

$$\begin{aligned} \Phi^{(T)}(x_n) &= \sum_{q=1}^{2H} [(\mathbf{w}_K)_q + \sum_{t=0}^{T-1} (\Delta \mathbf{w}_K^{(t)})_q] (\mathbf{y}_{K-1,n}^{(T)})_q = \overbrace{\sum_{q=1}^{2H} (\mathbf{w}_K)_q (\mathbf{y}_{K-1,n}^{(T)})_q}^{=Y} + \overbrace{\sum_{q=1}^{2H} \sum_{t=0}^{T-1} (\Delta \mathbf{w}_K^{(t)})_q (\mathbf{y}_{K-1,n}^{(T)})_q}^{=S} \\ &= Y + S. \end{aligned} \quad (5)$$

where  $(\mathbf{w}_K)_q \sim \mathcal{N}(0, \frac{\alpha}{2H})$ ;  $n \in \{N+1, \dots, N+\tilde{N}\}$ ; and  $Y$  and  $S$  are continuous RVs, as defined on the top of this page. By plugging (5) into the RHS of [2, eq. (41)], the probability of point misclassification error  $P_e$  manifested by  $\Phi^{(T)}$  becomes

$$P_e = (P_e|\mathcal{H}_{-1} + P_e|\mathcal{H}_1)/2, \quad (6)$$

where

$$P_e|\mathcal{H}_{-1} = \mathbb{P}(Y + S > 0|\mathcal{H}_{-1}) = \mathbb{P}(Y|\mathcal{H}_{-1} > -S|\mathcal{H}_{-1}) \quad (7a)$$

$$P_e|\mathcal{H}_1 = \mathbb{P}(Y + S < 0|\mathcal{H}_1) = \mathbb{P}(Y|\mathcal{H}_1 < -S|\mathcal{H}_1). \quad (7b)$$

To derive  $P_e|\mathcal{H}_{-1}$  from the RHS of (7a), we first underscore that  $S|\mathcal{H}_{-1}$  – as defined in (5) – is a continuous RV that can take values in  $(-\infty, \infty)$  with some probability. Thus, we can condition

on the continuous random values of  $S|\mathcal{H}_{-1}$  while employing the law of total probability for a continuous case [2, Law 2] to simplify the RHS of (7a) as follows:

$$P_e|\mathcal{H}_{-1} = \mathbb{P}(Y|\mathcal{H}_{-1} > -S|\mathcal{H}_{-1}) \quad (8a)$$

$$\stackrel{(a)}{=} \int_{-\infty}^{\infty} \mathbb{P}(Y|\mathcal{H}_{-1} > -S_{-1}|S_{-1} = s) f_{S_{-1}}(s) ds \quad (8b)$$

$$= \int_{-\infty}^{\infty} \mathbb{P}(Y|\mathcal{H}_{-1} > -s) f_{S_{-1}}(s) ds, \quad (8c)$$

where  $S_{-1} := S|\mathcal{H}_{-1}$ ; (a) follows from [2, eq. (19)] w.r.t. an event  $\mathcal{A} := \{Y|\mathcal{H}_{-1} > -S|\mathcal{H}_{-1}\}$ ; and  $f_{S_{-1}}$  is the probability density function (PDF) of  $S_{-1} := S|\mathcal{H}_{-1}$ . Meanwhile, as for  $\mathbf{y}_{K-1,n}^{(T)} = [(\mathbf{y}_{K-1,n}^{(T)})_1, (\mathbf{y}_{K-1,n}^{(T)})_2, \dots, (\mathbf{y}_{K-1,n}^{(T)})_{2H}]^\top \in \mathbb{R}_+^{2H}$ , let  $y_{\max|\mathcal{H}_{-1}} := \max((\mathbf{y}_{K-1,n}^{(T)})_1|\mathcal{H}_{-1}, (\mathbf{y}_{K-1,n}^{(T)})_2|\mathcal{H}_{-1}, \dots, (\mathbf{y}_{K-1,n}^{(T)})_{2H}|\mathcal{H}_{-1})$  for  $y_{\max|\mathcal{H}_{-1}} \in \mathbb{R}_+$ . It then follows via (5) that  $Y|\mathcal{H}_{-1} \leq y_{\max|\mathcal{H}_{-1}} \times \sum_{q=1}^{2H} (\mathbf{w}_K)_q - (\mathbf{w}_K)_q \sim \mathcal{N}(0, \frac{\alpha}{2H})$  and  $\forall q \in [2H]$ . If we now let  $U := \sum_{q=1}^{2H} (\mathbf{w}_K)_q$ , the sum of  $2H$  independent Gaussian RVs, then  $U \sim \mathcal{N}(0, \alpha)$ . Hence,

$$\mathbb{P}(Y|\mathcal{H}_{-1} > -s) \leq \mathbb{P}(y_{\max|\mathcal{H}_{-1}} \times U > -s) \quad (9a)$$

$$= \mathbb{P}(U > -s/y_{\max|\mathcal{H}_{-1}}) \quad (9b)$$

$$= \frac{1}{\sqrt{\alpha}\sqrt{2\pi}} \int_{-s/y_{\max|\mathcal{H}_{-1}}}^{\infty} e^{-y^2/2\alpha} dy \quad (9c)$$

$$\stackrel{(a)}{=} \frac{1}{\sqrt{2\pi}} \int_{-s/(\sqrt{\alpha}y_{\max|\mathcal{H}_{-1}})}^{\infty} e^{-t^2/2} dt \quad (9d)$$

$$\stackrel{(b)}{=} \mathcal{Q}\left(-\frac{s}{\sqrt{\alpha}y_{\max|\mathcal{H}_{-1}}}\right), \quad (9e)$$

where (a) follows from integration by substitution w.r.t.  $t = y/\sqrt{\alpha}$  and hence  $dt = dy/\sqrt{\alpha}$ ; (b) follows from the definition of the  $\mathcal{Q}$ -function. Substituting (9e) into the RHS of (8c) then produces the expression

$$P_e|\mathcal{H}_{-1} \leq \int_{-\infty}^{\infty} \mathcal{Q}\left(-\frac{s}{\sqrt{\alpha}y_{\max|\mathcal{H}_{-1}}}\right) f_{S_{-1}}(s) ds. \quad (10)$$

Similarly, it follows from the RHS of (7b) and the law of total probability for a continuous case [2, Law 2] that:

$$P_e|\mathcal{H}_1 = \mathbb{P}(Y|\mathcal{H}_1 < -S|\mathcal{H}_1) \quad (11a)$$

$$\stackrel{(a)}{=} \int_{-\infty}^{\infty} \mathbb{P}(Y|\mathcal{H}_1 < -S_1|S_1 = s) f_{S_1}(s) ds \quad (11b)$$

$$= \int_{-\infty}^{\infty} \mathbb{P}(Y|\mathcal{H}_1 < -s) f_{S_1}(s) ds, \quad (11c)$$

where  $S_1 := S|\mathcal{H}_1$ ; (a) is due to [2, eq. (19)] w.r.t. an event  $\mathcal{A} := \{Y|\mathcal{H}_1 < -S|\mathcal{H}_1\}$ ;  $f_{S_1}$  is the PDF of  $S_1 := S|\mathcal{H}_1$ . To simplify the RHS of (11c) by simplifying  $\mathbb{P}(Y|\mathcal{H}_1 < -s)$ , let  $y_{\min|\mathcal{H}_1} := \min((\mathbf{y}_{K-1,n}^{(T)})_1|\mathcal{H}_1,$



$(\mathbf{y}_{K-1,n}^{(T)})_2 | \mathcal{H}_1, \dots, (\mathbf{y}_{K-1,n}^{(T)})_{2H} | \mathcal{H}_1 \in \mathbb{R}_+$ . It then ensues via (5) that  $Y | \mathcal{H}_1 \geq y_{\min | \mathcal{H}_1} \times \sum_{q=1}^{2H} (\mathbf{w}_K)_q$  for  $(\mathbf{w}_K)_q \sim \mathcal{N}(0, \frac{\alpha}{2H})$  and  $\forall q \in [2H]$ . If we now let  $U := \sum_{q=1}^{2H} (\mathbf{w}_K)_q$ , then  $U \sim \mathcal{N}(0, \alpha)$  and thus:

$$\mathbb{P}(Y | \mathcal{H}_1 < -s) \leq \mathbb{P}(y_{\min | \mathcal{H}_1} \times U < -s) \quad (12a)$$

$$= \mathbb{P}(U < -s/y_{\min | \mathcal{H}_1}) \quad (12b)$$

$$= \frac{1}{\sqrt{\alpha}\sqrt{2\pi}} \int_{-\infty}^{-s/y_{\min | \mathcal{H}_1}} e^{-y^2/2\alpha} dy \quad (12c)$$

$$\stackrel{(a)}{=} \frac{1}{\sqrt{2\pi}} \int_{s/(\sqrt{\alpha}y_{\min | \mathcal{H}_1})}^{\infty} e^{-t^2/2} dt \quad (12d)$$

$$\stackrel{(b)}{=} \mathcal{Q}\left(\frac{s}{\sqrt{\alpha}y_{\min | \mathcal{H}_1}}\right), \quad (12e)$$

where (a) follows from integration by substitution w.r.t.  $t = -y/\sqrt{\alpha}$  and hence  $dt = -dy/\sqrt{\alpha}$ ; (b) follows from the definition of the  $\mathcal{Q}$ -function. Substituting (12e) into the RHS of (11c) then gives

$$P_e | \mathcal{H}_1 \leq \int_{-\infty}^{\infty} \mathcal{Q}\left(\frac{s}{\sqrt{\alpha}y_{\min | \mathcal{H}_1}}\right) f_{S_1}(s) ds. \quad (13)$$

Plugging (13) and (10) into the RHS of (6) produces

$$P_e \leq \frac{1}{2} \int_{-\infty}^{\infty} \left[ \mathcal{Q}\left(-\frac{s}{\sqrt{\alpha}y_{\max | \mathcal{H}_{-1}}}\right) f_{S_{-1}}(s) + \mathcal{Q}\left(\frac{s}{\sqrt{\alpha}y_{\min | \mathcal{H}_1}}\right) f_{S_1}(s) \right] ds. \quad (14)$$

To reveal the asymptotic behavior of the RHS of (14) and upper bound on the exhibited  $P_e$ , we are going to study two major cases when  $(y_{\max | \mathcal{H}_{-1}}, y_{\min | \mathcal{H}_1}) \rightarrow (\infty, \infty)$  and  $(y_{\max | \mathcal{H}_{-1}}, y_{\min | \mathcal{H}_1}) \rightarrow (0, \infty)$ . Beginning with the former, as  $(y_{\max | \mathcal{H}_{-1}}, y_{\min | \mathcal{H}_1}) \rightarrow (\infty, \infty)$ , it follows via these constants' definitions that  $(\|\mathbf{y}_{K-1,n}^{(T)}\| | \mathcal{H}_{-1}, \|\mathbf{y}_{K-1,n}^{(T)}\| | \mathcal{H}_1) \rightarrow (\infty, \infty)$  and thus  $\|\mathbf{y}_{K-1,n}^{(T)}\| \rightarrow \infty$ . Accordingly,

$$\lim_{\|\mathbf{y}_{K-1,n}^{(T)}\| \rightarrow \infty} P_e = \lim_{(y_{\max | \mathcal{H}_{-1}}, y_{\min | \mathcal{H}_1}) \rightarrow (\infty, \infty)} P_e. \quad (15)$$

Deploying (14) in the RHS of (15) followed by applying the limit and its properties produce

$$\begin{aligned} \lim_{\|\mathbf{y}_{K-1,n}^{(T)}\| \rightarrow \infty} P_e &\leq \frac{1}{2} \int_{-\infty}^{\infty} \left[ \lim_{y_{\max | \mathcal{H}_{-1}} \rightarrow \infty} \mathcal{Q}\left(-\frac{s}{\sqrt{\alpha}y_{\max | \mathcal{H}_{-1}}}\right) \times \lim_{(y_{\max | \mathcal{H}_{-1}}, y_{\min | \mathcal{H}_1}) \rightarrow (\infty, \infty)} f_{S_{-1}}(s) \right. \\ &\quad \left. + \lim_{y_{\min | \mathcal{H}_1} \rightarrow \infty} \mathcal{Q}\left(\frac{s}{\sqrt{\alpha}y_{\min | \mathcal{H}_1}}\right) \times \lim_{(y_{\max | \mathcal{H}_{-1}}, y_{\min | \mathcal{H}_1}) \rightarrow (\infty, \infty)} f_{S_1}(s) \right] ds. \end{aligned} \quad (16)$$

Meanwhile, the properties of the  $\mathcal{Q}$ -function and limit lead to the following:

$$\lim_{y_{\max | \mathcal{H}_{-1}} \rightarrow \infty} \mathcal{Q}\left(-\frac{s}{\sqrt{\alpha}y_{\max | \mathcal{H}_{-1}}}\right) \stackrel{(a)}{=} \mathcal{Q}(0) \stackrel{(b)}{=} 1/2 \quad (17a)$$

$$\lim_{y_{\min | \mathcal{H}_1} \rightarrow \infty} \mathcal{Q}\left(\frac{s}{\sqrt{\alpha}y_{\min | \mathcal{H}_1}}\right) \stackrel{(a)}{=} \mathcal{Q}(0) \stackrel{(b)}{=} 1/2, \quad (17b)$$

where (a) is for any  $s \in (-\infty, \infty)$ ; (b) is for the  $\mathcal{Q}$ -function's property. Plugging (17a)&(17b) into the RHS of (16),

$$\lim_{\|\mathbf{y}_{K-1,n}^{(T)}\| \rightarrow \infty} P_e \leq \lim_{(y_{\max | \mathcal{H}_{-1}}, y_{\min | \mathcal{H}_1}) \rightarrow (\infty, \infty)} \left[ \int_{-\infty}^{\infty} f_{S_{-1}}(s) ds + \int_{-\infty}^{\infty} f_{S_1}(s) ds \right] \times 1/4 \stackrel{(a)}{=} 1/2, \quad (18)$$

where (a) is for  $\int_{-\infty}^{\infty} f_{S_{-1}}(s) ds = \int_{-\infty}^{\infty} f_{S_1}(s) ds = 1$ . This proves (2a).  $\square$

To prove (2b), we first decompose the RHS of (14) into the sum of four summands that constitute an expression given by

$$P_e \leq \frac{1}{2} \int_{-\infty}^0 \left[ \mathcal{Q}\left(-\frac{s}{\sqrt{\alpha}y_{\max|\mathcal{H}_{-1}}}\middle|s < 0\right) f_{S_{-1}}(s) + \mathcal{Q}\left(\frac{s}{\sqrt{\alpha}y_{\min|\mathcal{H}_1}}\middle|s < 0\right) f_{S_1}(s) \right] ds + \\ \frac{1}{2} \int_0^{\infty} \left[ \mathcal{Q}\left(-\frac{s}{\sqrt{\alpha}y_{\max|\mathcal{H}_{-1}}}\middle|s > 0\right) f_{S_{-1}}(s) + \mathcal{Q}\left(\frac{s}{\sqrt{\alpha}y_{\min|\mathcal{H}_1}}\middle|s > 0\right) f_{S_1}(s) \right] ds. \quad (19)$$

Proceeding to the second case, as  $(y_{\max|\mathcal{H}_{-1}}, y_{\min|\mathcal{H}_1}) \rightarrow (0, \infty)$ ,  $(\|\mathbf{y}_{K-1,n}^{(T)}\|\|\mathcal{H}_{-1}\|, \|\mathbf{y}_{K-1,n}^{(T)}\|\|\mathcal{H}_1\|) \rightarrow (0, \infty)$ . As a result,

$$\lim_{(\|\mathbf{y}_{K-1,n}^{(T)}\|\|\mathcal{H}_{-1}\|, \|\mathbf{y}_{K-1,n}^{(T)}\|\|\mathcal{H}_1\|) \rightarrow (0, \infty)} P_e = \lim_{(y_{\max|\mathcal{H}_{-1}}, y_{\min|\mathcal{H}_1}) \rightarrow (0, \infty)} P_e. \quad (20)$$

Plugging (19) into the RHS of (20) and applying the limit and its properties yield

$$\lim_{(\|\mathbf{y}_{K-1,n}^{(T)}\|\|\mathcal{H}_{-1}\|, \|\mathbf{y}_{K-1,n}^{(T)}\|\|\mathcal{H}_1\|) \rightarrow (0, \infty)} P_e \leq \frac{1}{2} \int_{-\infty}^0 \left[ \lim_{y_{\max|\mathcal{H}_{-1}} \rightarrow 0} \mathcal{Q}\left(-\frac{s}{\sqrt{\alpha}y_{\max|\mathcal{H}_{-1}}}\middle|s < 0\right) \right. \\ \times \lim_{(y_{\max|\mathcal{H}_{-1}}, y_{\min|\mathcal{H}_1}) \rightarrow (0, \infty)} f_{S_{-1}}(s) + \lim_{y_{\min|\mathcal{H}_1} \rightarrow \infty} \mathcal{Q}\left(\frac{s}{\sqrt{\alpha}y_{\min|\mathcal{H}_1}}\middle|s < 0\right) \times \lim_{(y_{\max|\mathcal{H}_{-1}}, y_{\min|\mathcal{H}_1}) \rightarrow (0, \infty)} f_{S_1}(s) \Big] ds \\ + \frac{1}{2} \int_0^{\infty} \left[ \lim_{y_{\max|\mathcal{H}_{-1}} \rightarrow 0} \mathcal{Q}\left(-\frac{s}{\sqrt{\alpha}y_{\max|\mathcal{H}_{-1}}}\middle|s > 0\right) \times \lim_{(y_{\max|\mathcal{H}_{-1}}, y_{\min|\mathcal{H}_1}) \rightarrow (0, \infty)} f_{S_{-1}}(s) \right. \\ \left. + \lim_{y_{\min|\mathcal{H}_1} \rightarrow \infty} \mathcal{Q}\left(\frac{s}{\sqrt{\alpha}y_{\min|\mathcal{H}_1}}\middle|s > 0\right) \times \lim_{(y_{\max|\mathcal{H}_{-1}}, y_{\min|\mathcal{H}_1}) \rightarrow (0, \infty)} f_{S_1}(s) \right] ds. \quad (21)$$

It follows from the  $\mathcal{Q}$ -function definition and limit properties w.r.t.  $\alpha \in \{1, 2\}$  and  $H < \infty$ :

$$\lim_{y_{\max|\mathcal{H}_{-1}} \rightarrow 0} \mathcal{Q}\left(-\frac{s}{\sqrt{\alpha}y_{\max|\mathcal{H}_{-1}}}\middle|s < 0\right) = \mathcal{Q}(\infty) = 0. \quad (22a)$$

$$\lim_{y_{\min|\mathcal{H}_1} \rightarrow \infty} \mathcal{Q}\left(\frac{s}{\sqrt{\alpha}y_{\min|\mathcal{H}_1}}\middle|s < 0\right) = \mathcal{Q}(0) = \frac{1}{2}. \quad (22b)$$

$$\lim_{y_{\max|\mathcal{H}_{-1}} \rightarrow 0} \mathcal{Q}\left(-\frac{s}{\sqrt{\alpha}y_{\max|\mathcal{H}_{-1}}}\middle|s > 0\right) = \mathcal{Q}(-\infty) = 1. \quad (22c)$$

$$\lim_{y_{\min|\mathcal{H}_1} \rightarrow \infty} \mathcal{Q}\left(\frac{s}{\sqrt{\alpha}y_{\min|\mathcal{H}_1}}\middle|s > 0\right) = \mathcal{Q}(0) = \frac{1}{2}. \quad (22d)$$

Substituting (22a)-(22d) into the RHS of (21) then gives (23).

$$\lim_{(\|\mathbf{y}_{K-1,n}^{(T)}\|\|\mathcal{H}_{-1}\|, \|\mathbf{y}_{K-1,n}^{(T)}\|\|\mathcal{H}_1\|) \rightarrow (0, \infty)} P_e \leq \frac{1}{2} \left[ \int_{-\infty}^0 \frac{1}{2} \times \lim_{(y_{\max|\mathcal{H}_{-1}}, y_{\min|\mathcal{H}_1}) \rightarrow (0, \infty)} f_{S_1}(s) ds + \right. \\ \left. \int_0^{\infty} \lim_{(y_{\max|\mathcal{H}_{-1}}, y_{\min|\mathcal{H}_1}) \rightarrow (0, \infty)} f_{S_{-1}}(s) ds + \int_0^{\infty} \frac{1}{2} \times \lim_{(y_{\max|\mathcal{H}_{-1}}, y_{\min|\mathcal{H}_1}) \rightarrow (0, \infty)} f_{S_1}(s) ds \right]. \quad (23)$$

Rearranging the first and third summands of (23); applying the properties of the limit; and exploiting the PDF identity  $\int_{-\infty}^{\infty} f_{S_1}(s) ds = 1$  lead to

$$\lim_{(\|\mathbf{y}_{K-1,n}^{(T)}\|\|\mathcal{H}_{-1}\|, \|\mathbf{y}_{K-1,n}^{(T)}\|\|\mathcal{H}_1\|) \rightarrow (0, \infty)} P_e \leq \frac{1}{2} \left[ \frac{1}{2} + \int_0^{\infty} \lim_{(y_{\max|\mathcal{H}_{-1}}, y_{\min|\mathcal{H}_1}) \rightarrow (0, \infty)} f_{S_{-1}}(s) ds \right], \quad (24)$$

where it follows from (5) that

$$S_{-1} := S|\mathcal{H}_{-1} = \sum_{q=1}^{2H} \sum_{t=0}^{T-1} (\Delta \mathbf{w}_K^{(t)})_q [(\mathbf{y}_{K-1,n}^{(T)})_q | \mathcal{H}_{-1}]. \quad (25)$$

As  $\|\mathbf{y}_{K-1,n}^{(T)}\|_{\mathcal{H}_{-1}} \rightarrow 0$ ,  $(\mathbf{y}_{K-1,n}^{(T)})_q |_{\mathcal{H}_{-1}} \rightarrow 0$ ,  $\forall q$  and  $n$ . Consequently, it follows via (25) that  $\lim_{(y_{\max}|\mathcal{H}_{-1}, y_{\min}|\mathcal{H}_1) \rightarrow (0, \infty)} f_{S-1}(s)$  becomes the Dirac delta function  $\delta(s)$ . Plugging  $\delta(s)$  into the RHS (24) produces

$$\lim_{(\|\mathbf{y}_{K-1,n}^{(T)}\|_{\mathcal{H}_{-1}}, \|\mathbf{y}_{K-1,n}^{(T)}\|_{\mathcal{H}_1}) \rightarrow (0, \infty)} P_e \leq \frac{1}{4} + \frac{1}{2} \int_0^\infty \delta(s) ds. \quad (26)$$

Because the PDF of  $\delta(s)$  gives an identity  $\int_{-\infty}^\infty \delta(s) ds = 1$  and  $\delta(s)$  is an even function [3],  $\int_0^\infty \delta(s) ds = 1/2$ . Substituting this value into the RHS of (26) produces

$$\lim_{(\|\mathbf{y}_{K-1,n}^{(T)}\|_{\mathcal{H}_{-1}}, \|\mathbf{y}_{K-1,n}^{(T)}\|_{\mathcal{H}_1}) \rightarrow (0, \infty)} P_e \leq 1/2. \quad (27)$$

As a result, (27) proves (2b). □

Therefore, (2a) and (2b) are now proven. This concludes the proof of Theorem 1. ■

### 3 PROOF OF THEOREM 2

**Theorem 2.** Let  $\check{\Phi}^{(T)} := [[\check{\mathbf{w}}_1^{(T)}, 0], [\check{\mathbf{W}}_2^{(T)}, 0], \dots, [\check{\mathbf{W}}_{K-1}^{(T)}, 0], [\check{\mathbf{w}}_K^{(T)}, 0]]$  – given  $\check{\mathbf{w}}_K^{(T)} \in \mathbb{R}^{1 \times 2H}$ ,  $\check{\mathbf{W}}_{K-k}^{(T)} \in \mathbb{R}^{2H \times 2H} \forall k \in [K-2]$ , and  $\check{\mathbf{w}}_1^{(T)} \in \mathbb{R}^{2H}$  – be a (deep) FNN with ReLU and Tanh activation trained over  $\mathcal{D} := \{(x_n, y_n)\}_{n=1}^N$  using hinge loss and SGD, SGD with momentum, RMSProp, or Adam after being initialized by a Gaussian initializer such as LeCun normal or He normal, and to be tested over  $\mathcal{T} := \{(x_n, y_n)\}_{n=N+1}^{N+\tilde{N}}$ , given  $H, K, N, \tilde{N}, T \in \mathbb{N}$ . For  $N, \tilde{N}, T, K \geq 2$  and  $H < \infty$ :

$$\lim_{\|\check{\mathbf{y}}_{K-1,n}^{(T)}\| \rightarrow \infty} \check{P}_e \leq 1/2 \quad (28a)$$

$$\lim_{(\|\check{\mathbf{y}}_{K-1,n}^{(T)}\|_{\mathcal{H}_{-1}}, \|\check{\mathbf{y}}_{K-1,n}^{(T)}\|_{\mathcal{H}_1}) \rightarrow (0, \infty)} \check{P}_e \leq 1/2, \quad (28b)$$

where (28a) and (28b) are true for all  $n \in \{N+1, \dots, N+\tilde{N}\}$ .

#### Proof of Theorem 2

It follows from [2, eq. (46)] and [2, eq. (30)] that

$$\check{P}_e = \frac{1}{2} [\mathbb{P}(\check{\Phi}^{(T)}(x_n) > 0 | \mathcal{H}_{-1}) + \mathbb{P}(\check{\Phi}^{(T)}(x_n) < 0 | \mathcal{H}_1)], \quad (29)$$

where  $\check{\Phi}^{(T)}(x_n) = \tanh(\check{\mathbf{w}}_K^{(T)} \check{\mathbf{y}}_{K-1,n}^{(T)})$ . Let us now consider

$$\theta = \check{\mathbf{w}}_K^{(T)} \check{\mathbf{y}}_{K-1,n}^{(T)} = \sum_{q=1}^{2H} (\check{\mathbf{w}}_K^{(T)})_q (\check{\mathbf{y}}_{K-1,n}^{(T)})_q, \quad (30)$$

where  $n \in \{N+1, \dots, N+\tilde{N}\}$  and it follows from [2, eq. (31)] for  $\check{\Sigma}_{1,n}^{(T)} = \text{diag}(\mathbb{I}\{\check{\mathbf{w}}_1^{(T)} x_n \geq 0\}) \in \{0, 1\}^{2H \times 2H}$  and  $\check{\Sigma}_{k,n}^{(T)} = \text{diag}(\mathbb{I}\{\check{\mathbf{W}}_k^{(T)} (\prod_{l=1}^{k-2} \check{\Sigma}_{k-l,n}^{(T)} \check{\mathbf{W}}_{k-l}^{(T)}) \check{\Sigma}_{1,n}^{(T)} \check{\mathbf{w}}_1^{(T)} x_n \geq 0\}) \in \{0, 1\}^{2H \times 2H}$  that

$$\check{\mathbf{y}}_{K-1,n}^{(T)} = \left( \prod_{k=1}^{K-2} \check{\Sigma}_{K-k,n}^{(T)} \check{\mathbf{W}}_{K-k}^{(T)} \right) \check{\Sigma}_{1,n}^{(T)} \check{\mathbf{w}}_1^{(T)} x_n \in \mathbb{R}_+^{2H}. \quad (31)$$

It then follows from (30) and the definition of the hyperbolic tangent function  $\tanh(\cdot)$  [4] that

$$\check{\Phi}^{(T)}(x_n) = \tanh(\theta) = \frac{e^\theta - e^{-\theta}}{e^\theta + e^{-\theta}} = \frac{e^{2\theta} - 1}{e^{2\theta} + 1}, \quad (32)$$

where  $\theta$  is given by (30). Employing (32) in the RHS of (29) leads to

$$\check{P}_e = \frac{1}{2} [\mathbb{P}(\tanh(\theta) > 0 | \mathcal{H}_{-1}) + \mathbb{P}(\tanh(\theta) < 0 | \mathcal{H}_1)]. \quad (33)$$

Using the equivalences in (32), the underlying probabilities can be simplified as follows

$$\mathbb{P}(\tanh(\theta) > 0) = \mathbb{P}\left(\frac{e^{2\theta} - 1}{e^{2\theta} + 1} > 0\right) = \mathbb{P}(e^{2\theta} > 1) \stackrel{(a)}{=} \mathbb{P}(\ln(e^{2\theta}) > \ln(1)) \stackrel{(b)}{=} \mathbb{P}(\theta > 0) \quad (34a)$$

$$\mathbb{P}(\tanh(\theta) < 0) = \mathbb{P}\left(\frac{e^{2\theta} - 1}{e^{2\theta} + 1} < 0\right) = \mathbb{P}(e^{2\theta} < 1) \stackrel{(a)}{=} \mathbb{P}(\ln(e^{2\theta}) < \ln(1)) \stackrel{(b)}{=} \mathbb{P}(\theta < 0), \quad (34b)$$

where (a) follows from applying the monotonically increasing function  $\ln(x)$  to both sides; (b) is due to the fact that  $\ln(e^{2\theta}) = 2\theta$  and  $\ln(1) = 1$ . Accordingly, it follows directly from (34a) and (34b) that

$$\mathbb{P}(\tanh(\theta) > 0 | \mathcal{H}_{-1}) = \mathbb{P}(\theta > 0 | \mathcal{H}_{-1}) \quad (35a)$$

$$\mathbb{P}(\tanh(\theta) < 0 | \mathcal{H}_1) = \mathbb{P}(\theta < 0 | \mathcal{H}_1). \quad (35b)$$

Meanwhile, substituting (35a) and (35b) into the RHS of (33) leads to the expression

$$\check{P}_e = \frac{1}{2} [\mathbb{P}(\theta > 0 | \mathcal{H}_{-1}) + \mathbb{P}(\theta < 0 | \mathcal{H}_1)], \quad (36)$$

where  $\theta$  is defined in (30). We now simplify  $\theta$  so as to simplify the RHS of (36).

The  $K$ -th FNN layer's weight vector at convergence  $\check{\mathbf{w}}_K^{(T)} \in \mathbb{R}^{1 \times 2H}$  can be expressed via [2, eq. (42c)] for all  $q \in [2H]$  as

$$(\check{\mathbf{w}}_K^{(T)})_q = (\check{\mathbf{w}}_K)_q + \sum_{t=0}^{T-1} (\Delta \check{\mathbf{w}}_K^{(t)})_q, \quad (37)$$

where  $(\check{\mathbf{w}}_K)_q := (\check{\mathbf{w}}_K^{(0)})_q$  is initialized with a Gaussian initializer such as LeCun normal or He normal (see [2, Definition 10]) and hence  $(\check{\mathbf{w}}_K)_q \sim \mathcal{N}(0, \alpha/2H)$  for  $\alpha \in \{1, 2\}$  ( $\alpha = 1$  for LeCun normal and  $\alpha = 2$  for He normal); and  $\Delta \check{\mathbf{w}}_K^{(t)}$  is the weight correction during the  $t$ -th iteration of SGD, SGD with momentum, RMSProp, or Adam. Meanwhile, substituting (37) into the RHS of (30) gives

$$\theta = \sum_{q=1}^{2H} \left[ (\check{\mathbf{w}}_K)_q + \sum_{t=0}^{T-1} (\Delta \check{\mathbf{w}}_K^{(t)})_q \right] (\check{\mathbf{y}}_{K-1,n}^{(T)})_q \quad (38a)$$

$$= \sum_{q=1}^{2H} (\check{\mathbf{w}}_K)_q (\check{\mathbf{y}}_{K-1,n}^{(T)})_q + \sum_{q=1}^{2H} \sum_{t=0}^{T-1} (\Delta \check{\mathbf{w}}_K^{(t)})_q (\check{\mathbf{y}}_{K-1,n}^{(T)})_q \quad (38b)$$

$$= \check{Y} + \check{S}, \quad (38c)$$

where  $(\check{\mathbf{w}}_K)_q \sim \mathcal{N}(0, \frac{\alpha}{2H})$ ;  $n \in \{N+1, \dots, N+\tilde{N}\}$ ; and  $\check{Y}$  and  $\check{S}$  are continuous RVs that have already been conditioned on a previously computed random vector  $\check{\mathbf{y}}_{K-1,n}^{(T)}$  and are defined as

$$\check{Y} = \sum_{q=1}^{2H} (\check{\mathbf{w}}_K)_q (\check{\mathbf{y}}_{K-1,n}^{(T)})_q \quad (39a)$$

$$\check{S} = \sum_{q=1}^{2H} \sum_{t=0}^{T-1} (\Delta \check{\mathbf{w}}_K^{(t)})_q (\check{\mathbf{y}}_{K-1,n}^{(T)})_q, \quad (39b)$$

where (a) follows from [2, eq. (31)]. By substituting (38c) into the RHS of (36), the probability of point misclassification error  $\check{P}_e$  manifested by  $\check{\Phi}^{(T)}$  can be equivalently expressed as

$$\check{P}_e = \frac{1}{2}(\check{P}_e|\mathcal{H}_{-1} + \check{P}_e|\mathcal{H}_1), \quad (40)$$

where

$$\check{P}_e|\mathcal{H}_{-1} = \mathbb{P}(\check{Y} + \check{S} > 0|\mathcal{H}_{-1}) = \mathbb{P}(\check{Y}|\mathcal{H}_{-1} > -\check{S}|\mathcal{H}_{-1}) \quad (41a)$$

$$\check{P}_e|\mathcal{H}_1 = \mathbb{P}(\check{Y} + \check{S} < 0|\mathcal{H}_1) = \mathbb{P}(\check{Y}|\mathcal{H}_1 < -\check{S}|\mathcal{H}_1). \quad (41b)$$

To derive  $\check{P}_e|\mathcal{H}_{-1}$  from the RHS of (41a), we first highlight that  $\check{S}|\mathcal{H}_{-1}$  is a continuous RV that can take values in  $(-\infty, \infty)$  per (39b). Hence, we can condition on the continuous random values of  $\check{S}|\mathcal{H}_{-1}$  while employing the law of total probability for a continuous case (see [2, Law 2]) to simplify the RHS of (41a) as follows:

$$\check{P}_e|\mathcal{H}_{-1} = \mathbb{P}(\check{Y}|\mathcal{H}_{-1} > -\check{S}|\mathcal{H}_{-1}) \stackrel{(a)}{=} \int_{-\infty}^{\infty} \mathbb{P}(\check{Y}|\mathcal{H}_{-1} > -\check{S}_{-1}|\check{S}_{-1} = s) f_{\check{S}_{-1}}(s) ds \quad (42a)$$

$$= \int_{-\infty}^{\infty} \mathbb{P}(\check{Y}|\mathcal{H}_{-1} > -s) f_{\check{S}_{-1}}(s) ds, \quad (42b)$$

where  $\check{S}_{-1} := \check{S}|\mathcal{H}_{-1}$ ; (a) follows from [2, eq. (19)] w.r.t. an event  $\mathcal{A} = \{\check{Y}|\mathcal{H}_{-1} > -\check{S}|\mathcal{H}_{-1}\}$ ; and  $f_{\check{S}_{-1}}$  is the probability density function (PDF) of  $\check{S}_{-1} := \check{S}|\mathcal{H}_{-1}$ .

As to  $\check{\mathbf{y}}_{K-1,n}^{(T)} = [(\check{\mathbf{y}}_{K-1,n}^{(T)})_1, (\check{\mathbf{y}}_{K-1,n}^{(T)})_2, \dots, (\check{\mathbf{y}}_{K-1,n}^{(T)})_{2H}]^\top \in \mathbb{R}_+^{2H}$ , let  $\check{y}_{\max|\mathcal{H}_{-1}} := \max((\check{\mathbf{y}}_{K-1,n}^{(T)})_1|\mathcal{H}_{-1}, (\check{\mathbf{y}}_{K-1,n}^{(T)})_2|\mathcal{H}_{-1}, \dots, (\check{\mathbf{y}}_{K-1,n}^{(T)})_{2H}|\mathcal{H}_{-1})$  for  $\check{y}_{\max|\mathcal{H}_{-1}} \in \mathbb{R}_+$ . It then follows through (39a) that  $\check{Y}|\mathcal{H}_{-1} \leq \check{y}_{\max|\mathcal{H}_{-1}} \times \sum_{q=1}^{2H} (\check{\mathbf{w}}_K)_q$  given  $(\check{\mathbf{w}}_K)_q \sim \mathcal{N}(0, \frac{\alpha}{2H})$ ,  $\forall q \in [2H]$ . If we now suppose  $\check{U} := \sum_{q=1}^{2H} (\check{\mathbf{w}}_K)_q$ , the sum of  $2H$  independent Gaussian RVs, then  $\check{U} \sim \mathcal{N}(0, \alpha)$ . Accordingly,

$$\mathbb{P}(\check{Y}|\mathcal{H}_{-1} > -s) \leq \mathbb{P}(\check{y}_{\max|\mathcal{H}_{-1}} \times \check{U} > -s) \quad (43a)$$

$$= \mathbb{P}(\check{U} > -s/\check{y}_{\max|\mathcal{H}_{-1}}) \quad (43b)$$

$$= \frac{1}{\sqrt{\alpha}\sqrt{2\pi}} \int_{-s/\check{y}_{\max|\mathcal{H}_{-1}}}^{\infty} e^{-y^2/2\alpha} dy \quad (43c)$$

$$\stackrel{(a)}{=} \frac{1}{\sqrt{2\pi}} \int_{-s/(\sqrt{\alpha}\check{y}_{\max|\mathcal{H}_{-1}})}^{\infty} e^{-t^2/2} dt \quad (43d)$$

$$\stackrel{(b)}{=} \mathcal{Q}\left(-\frac{s}{\sqrt{\alpha}\check{y}_{\max|\mathcal{H}_{-1}}}\right), \quad (43e)$$

where (a) follows from integration by substitution w.r.t.  $t = y/\sqrt{\alpha}$  and hence  $dt = dy/\sqrt{\alpha}$ ; (b) follows from the definition of the  $\mathcal{Q}$ -function. Substituting (43e) into the RHS of (42b) then gives

$$\check{P}_e|\mathcal{H}_{-1} \leq \int_{-\infty}^{\infty} \mathcal{Q}\left(-\frac{s}{\sqrt{\alpha}\check{y}_{\max|\mathcal{H}_{-1}}}\right) f_{\check{S}_{-1}}(s) ds. \quad (44)$$

Similarly, it follows from the RHS of (41b) and the law of total probability for a continuous case [2, Law 2] that

$$\check{P}_e|\mathcal{H}_1 = \mathbb{P}(\check{Y}|\mathcal{H}_1 < -\check{S}|\mathcal{H}_1) \stackrel{(a)}{=} \int_{-\infty}^{\infty} \mathbb{P}(\check{Y}|\mathcal{H}_1 < -\check{S}_1|\check{S}_1 = s) f_{\check{S}_1}(s) ds \quad (45a)$$

$$= \int_{-\infty}^{\infty} \mathbb{P}(\check{Y}|\mathcal{H}_1 < -s) f_{\check{S}_1}(s) ds, \quad (45b)$$

where  $\check{S}_1 := \check{S}|\mathcal{H}_1$ ; (a) follows from [2, eq. (19)] w.r.t. an event  $\mathcal{A} := \{\check{Y}|\mathcal{H}_1 < -\check{S}|\mathcal{H}_1\}$ ; and  $f_{\check{S}_1}$  is the PDF of  $\check{S}_1 = \check{S}|\mathcal{H}_1$ . To simplify the RHS of (45b) via the simplification of  $\mathbb{P}(\check{Y}|\mathcal{H}_1 < -s)$ , let

us consider a constant  $\check{y}_{\min|\mathcal{H}_1} := \min((\check{\mathbf{y}}_{K-1,n}^{(T)})_1|\mathcal{H}_1, (\check{\mathbf{y}}_{K-1,n}^{(T)})_2|\mathcal{H}_1, \dots, (\check{\mathbf{y}}_{K-1,n}^{(T)})_{2H}|\mathcal{H}_1) \in \mathbb{R}_+$ . It then follows through (38c) that  $\check{Y}|\mathcal{H}_1 \geq \check{y}_{\min|\mathcal{H}_1} \times \sum_{q=1}^{2H} (\check{\mathbf{w}}_K)_q$  given  $(\check{\mathbf{w}}_K)_q \sim \mathcal{N}(0, \frac{\alpha}{2H})$ ,  $\forall q \in [2H]$ . If we now let  $\check{U} := \sum_{q=1}^{2H} (\check{\mathbf{w}}_K)_q$ , then  $\check{U} \sim \mathcal{N}(0, \alpha)$  and hence:

$$\mathbb{P}(\check{Y}|\mathcal{H}_1 < -s) \leq \mathbb{P}(\check{y}_{\min|\mathcal{H}_1} \times \check{U} < -s) \quad (46a)$$

$$= \mathbb{P}(\check{U} < -s/\check{y}_{\min|\mathcal{H}_1}) \quad (46b)$$

$$= \frac{1}{\sqrt{\alpha}\sqrt{2\pi}} \int_{-\infty}^{-s/\check{y}_{\min|\mathcal{H}_1}} e^{-y^2/2\alpha} dy \quad (46c)$$

$$\stackrel{(a)}{=} \frac{1}{\sqrt{2\pi}} \int_{s/(\sqrt{\alpha}\check{y}_{\min|\mathcal{H}_1})}^{\infty} e^{-t^2/2} dt \quad (46d)$$

$$\stackrel{(b)}{=} \mathcal{Q}\left(\frac{s}{\sqrt{\alpha}\check{y}_{\min|\mathcal{H}_1}}\right), \quad (46e)$$

where (a) follows from integration by substitution w.r.t.  $t = -y/\sqrt{\alpha}$  and hence  $dt = -dy/\sqrt{\alpha}$ ; (b) follows from the  $\mathcal{Q}$ -function's definition. Hence, substituting (46e) into the RHS of (45b) gives

$$\check{P}_e|\mathcal{H}_1 \leq \int_{-\infty}^{\infty} \mathcal{Q}\left(\frac{s}{\sqrt{\alpha}\check{y}_{\min|\mathcal{H}_1}}\right) f_{\check{S}_1}(s) ds. \quad (47)$$

As a result, substituting (47) and (44) into the RHS of (40) leads to

$$\check{P}_e \leq \frac{1}{2} \int_{-\infty}^{\infty} \left[ \mathcal{Q}\left(-\frac{s}{\sqrt{\alpha}\check{y}_{\max|\mathcal{H}_{-1}}}\right) f_{\check{S}_{-1}}(s) + \mathcal{Q}\left(\frac{s}{\sqrt{\alpha}\check{y}_{\min|\mathcal{H}_1}}\right) f_{\check{S}_1}(s) \right] ds. \quad (48)$$

where it follows from (39b) that

$$\check{S}_{-1} := \check{S}|\mathcal{H}_{-1} = \sum_{q=1}^{2H} \sum_{t=0}^{T-1} (\Delta \check{\mathbf{w}}_K^{(t)})_q [(\check{\mathbf{y}}_{K-1,n}^{(T)})_q|\mathcal{H}_{-1}] \quad (49a)$$

$$\check{S}_1 := \check{S}|\mathcal{H}_1 = \sum_{q=1}^{2H} \sum_{t=0}^{T-1} (\Delta \check{\mathbf{w}}_K^{(t)})_q [(\check{\mathbf{y}}_{K-1,n}^{(T)})_q|\mathcal{H}_1]. \quad (49b)$$

To uncover the asymptotic characteristics of the RHS of (48) and upper bound on the exhibited  $P_e$ , we are going to investigate two major cases: i.e.,  $(\check{y}_{\max|\mathcal{H}_{-1}}, \check{y}_{\min|\mathcal{H}_1}) \rightarrow (\infty, \infty)$  and  $(\check{y}_{\max|\mathcal{H}_{-1}}, \check{y}_{\min|\mathcal{H}_1}) \rightarrow (0, \infty)$ . Beginning with the former, as  $(\check{y}_{\max|\mathcal{H}_{-1}}, \check{y}_{\min|\mathcal{H}_1}) \rightarrow (\infty, \infty)$ , it follows through the definitions of these constants that  $(\|\check{\mathbf{y}}_{K-1,n}^{(T)}\|_{\mathcal{H}_{-1}}, \|\check{\mathbf{y}}_{K-1,n}^{(T)}\|_{\mathcal{H}_1}) \rightarrow (\infty, \infty)$  and hence  $\|\check{\mathbf{y}}_{K-1,n}^{(T)}\| \rightarrow \infty$ . Consequently,

$$\lim_{\|\check{\mathbf{y}}_{K-1,n}^{(T)}\| \rightarrow \infty} \check{P}_e = \lim_{(\check{y}_{\max|\mathcal{H}_{-1}}, \check{y}_{\min|\mathcal{H}_1}) \rightarrow (\infty, \infty)} \check{P}_e. \quad (50)$$

Deploying (48) in the RHS of (50) and applying the limit and its properties produce

$$\begin{aligned} \lim_{\|\check{\mathbf{y}}_{K-1,n}^{(T)}\| \rightarrow \infty} \check{P}_e &\leq \frac{1}{2} \int_{-\infty}^{\infty} \left[ \lim_{\check{y}_{\max|\mathcal{H}_{-1}} \rightarrow \infty} \mathcal{Q}\left(-\frac{s}{\sqrt{\alpha}\check{y}_{\max|\mathcal{H}_{-1}}}\right) \times \lim_{(\check{y}_{\max|\mathcal{H}_{-1}}, \check{y}_{\min|\mathcal{H}_1}) \rightarrow (\infty, \infty)} f_{\check{S}_{-1}}(s) \right. \\ &\quad \left. + \lim_{\check{y}_{\min|\mathcal{H}_1} \rightarrow \infty} \mathcal{Q}\left(\frac{s}{\sqrt{\alpha}\check{y}_{\min|\mathcal{H}_1}}\right) \times \lim_{(\check{y}_{\max|\mathcal{H}_{-1}}, \check{y}_{\min|\mathcal{H}_1}) \rightarrow (\infty, \infty)} f_{\check{S}_1}(s) \right] ds. \end{aligned} \quad (51)$$

In the meantime, the properties of the  $\mathcal{Q}$ -function and limit lead to:

$$\lim_{\check{y}_{\max|\mathcal{H}_{-1}} \rightarrow \infty} \mathcal{Q}\left(-\frac{s}{\sqrt{\alpha}\check{y}_{\max|\mathcal{H}_{-1}}}\right) \stackrel{(a)}{=} \mathcal{Q}(0) \stackrel{(b)}{=} 1/2 \quad (52a)$$

$$\lim_{\check{y}_{\min|\mathcal{H}_1} \rightarrow \infty} \mathcal{Q}\left(\frac{s}{\sqrt{\alpha}\check{y}_{\min|\mathcal{H}_1}}\right) \stackrel{(a)}{=} \mathcal{Q}(0) \stackrel{(b)}{=} 1/2, \quad (52b)$$

where (a) is valid for any  $s \in (-\infty, \infty)$  and (b) is due to the property of the  $Q$ -function. Substituting (52a)&(52b) into the RHS of (51),

$$\lim_{\|\tilde{\mathbf{y}}_{K-1,n}^{(T)}\| \rightarrow \infty} \check{P}_e \leq \lim_{(\tilde{y}_{\max|\mathcal{H}_{-1}}, \tilde{y}_{\min|\mathcal{H}_1}) \rightarrow (\infty, \infty)} \left[ \int_{-\infty}^{\infty} f_{\check{s}_{-1}}(s) ds + \int_{-\infty}^{\infty} f_{\check{s}_1}(s) ds \right] \times 1/4 \stackrel{(a)}{=} 1/2, \quad (53)$$

where (a) is due to the PDF property that  $\int_{-\infty}^{\infty} f_{\check{s}_{-1}}(s) ds = \int_{-\infty}^{\infty} f_{\check{s}_1}(s) ds = 1$ . This proves (28a).  $\square$

To prove (28b), we first decompose the RHS of (48) into the sum of four summands that constitute an expression given by

$$\begin{aligned} \check{P}_e \leq & \frac{1}{2} \int_{-\infty}^0 \left[ \mathcal{Q}\left(-\frac{s}{\sqrt{\alpha}\tilde{y}_{\max|\mathcal{H}_{-1}}}\middle|s < 0\right) f_{\check{s}_{-1}}(s) + \mathcal{Q}\left(\frac{s}{\sqrt{\alpha}\tilde{y}_{\min|\mathcal{H}_1}}\middle|s < 0\right) f_{\check{s}_1}(s) \right] ds + \\ & \frac{1}{2} \int_0^{\infty} \left[ \mathcal{Q}\left(-\frac{s}{\sqrt{\alpha}\tilde{y}_{\max|\mathcal{H}_{-1}}}\middle|s > 0\right) f_{\check{s}_{-1}}(s) + \mathcal{Q}\left(\frac{s}{\sqrt{\alpha}\tilde{y}_{\min|\mathcal{H}_1}}\middle|s > 0\right) f_{\check{s}_1}(s) \right] ds. \end{aligned} \quad (54)$$

Moving on to the second case, as  $(\tilde{y}_{\max|\mathcal{H}_{-1}}, \tilde{y}_{\min|\mathcal{H}_1}) \rightarrow (0, \infty)$ ,  $(\|\tilde{\mathbf{y}}_{K-1,n}^{(T)}\|\mathcal{H}_{-1}, \|\tilde{\mathbf{y}}_{K-1,n}^{(T)}\|\mathcal{H}_1) \rightarrow (0, \infty)$ . Consequently,

$$\lim_{(\|\tilde{\mathbf{y}}_{K-1,n}^{(T)}\|\mathcal{H}_{-1}, \|\tilde{\mathbf{y}}_{K-1,n}^{(T)}\|\mathcal{H}_1) \rightarrow (0, \infty)} \check{P}_e = \lim_{(\tilde{y}_{\max|\mathcal{H}_{-1}}, \tilde{y}_{\min|\mathcal{H}_1}) \rightarrow (0, \infty)} \check{P}_e. \quad (55)$$

Substituting (54) into the RHS of (55) and applying the limit and its properties give

$$\begin{aligned} \lim_{(\|\tilde{\mathbf{y}}_{K-1,n}^{(T)}\|\mathcal{H}_{-1}, \|\tilde{\mathbf{y}}_{K-1,n}^{(T)}\|\mathcal{H}_1) \rightarrow (0, \infty)} \check{P}_e \leq & \frac{1}{2} \int_{-\infty}^0 \left[ \lim_{\tilde{y}_{\max|\mathcal{H}_{-1}} \rightarrow 0} \mathcal{Q}\left(-\frac{s}{\sqrt{\alpha}\tilde{y}_{\max|\mathcal{H}_{-1}}}\middle|s < 0\right) \times \right. \\ & \lim_{(\tilde{y}_{\max|\mathcal{H}_{-1}}, \tilde{y}_{\min|\mathcal{H}_1}) \rightarrow (0, \infty)} f_{\check{s}_{-1}}(s) + \lim_{\tilde{y}_{\min|\mathcal{H}_1} \rightarrow \infty} \mathcal{Q}\left(\frac{s}{\sqrt{\alpha}\tilde{y}_{\min|\mathcal{H}_1}}\middle|s < 0\right) \times \lim_{(\tilde{y}_{\max|\mathcal{H}_{-1}}, \tilde{y}_{\min|\mathcal{H}_1}) \rightarrow (0, \infty)} f_{\check{s}_1}(s) \Big] ds \\ & + \frac{1}{2} \int_0^{\infty} \left[ \lim_{\tilde{y}_{\max|\mathcal{H}_{-1}} \rightarrow 0} \mathcal{Q}\left(-\frac{s}{\sqrt{\alpha}\tilde{y}_{\max|\mathcal{H}_{-1}}}\middle|s > 0\right) \times \lim_{(\tilde{y}_{\max|\mathcal{H}_{-1}}, \tilde{y}_{\min|\mathcal{H}_1}) \rightarrow (0, \infty)} f_{\check{s}_{-1}}(s) \right. \\ & \left. + \lim_{\tilde{y}_{\min|\mathcal{H}_1} \rightarrow \infty} \mathcal{Q}\left(\frac{s}{\sqrt{\alpha}\tilde{y}_{\min|\mathcal{H}_1}}\middle|s > 0\right) \times \lim_{(\tilde{y}_{\max|\mathcal{H}_{-1}}, \tilde{y}_{\min|\mathcal{H}_1}) \rightarrow (0, \infty)} f_{\check{s}_1}(s) \right] ds. \end{aligned} \quad (56)$$

It then follows from the  $Q$ -function definition and the limit properties w.r.t.  $\alpha \in \{1, 2\}$  and  $H < \infty$ :

$$\lim_{\tilde{y}_{\max|\mathcal{H}_{-1}} \rightarrow 0} \mathcal{Q}\left(-\frac{s}{\sqrt{\alpha}\tilde{y}_{\max|\mathcal{H}_{-1}}}\middle|s < 0\right) = \mathcal{Q}(\infty) = 0. \quad (57a)$$

$$\lim_{\tilde{y}_{\min|\mathcal{H}_1} \rightarrow \infty} \mathcal{Q}\left(\frac{s}{\sqrt{\alpha}\tilde{y}_{\min|\mathcal{H}_1}}\middle|s < 0\right) = \mathcal{Q}(0) = \frac{1}{2}. \quad (57b)$$

$$\lim_{\tilde{y}_{\max|\mathcal{H}_{-1}} \rightarrow 0} \mathcal{Q}\left(-\frac{s}{\sqrt{\alpha}\tilde{y}_{\max|\mathcal{H}_{-1}}}\middle|s > 0\right) = \mathcal{Q}(-\infty) = 1. \quad (57c)$$

$$\lim_{\tilde{y}_{\min|\mathcal{H}_1} \rightarrow \infty} \mathcal{Q}\left(\frac{s}{\sqrt{\alpha}\tilde{y}_{\min|\mathcal{H}_1}}\middle|s > 0\right) = \mathcal{Q}(0) = \frac{1}{2}. \quad (57d)$$

Replacing (57a)-(57d) into the RHS of (56) then gives

$$\begin{aligned} \lim_{(\|\tilde{\mathbf{y}}_{K-1,n}^{(T)}\|\mathcal{H}_{-1}, \|\tilde{\mathbf{y}}_{K-1,n}^{(T)}\|\mathcal{H}_1) \rightarrow (0, \infty)} \check{P}_e \leq & \frac{1}{2} \left[ \int_{-\infty}^0 \frac{1}{2} \times \lim_{(\tilde{y}_{\max|\mathcal{H}_{-1}}, \tilde{y}_{\min|\mathcal{H}_1}) \rightarrow (0, \infty)} f_{\check{s}_1}(s) ds + \right. \\ & \left. \int_0^{\infty} \lim_{(\tilde{y}_{\max|\mathcal{H}_{-1}}, \tilde{y}_{\min|\mathcal{H}_1}) \rightarrow (0, \infty)} f_{\check{s}_{-1}}(s) ds + \int_0^{\infty} \frac{1}{2} \times \lim_{(\tilde{y}_{\max|\mathcal{H}_{-1}}, \tilde{y}_{\min|\mathcal{H}_1}) \rightarrow (0, \infty)} f_{\check{s}_1}(s) ds \right]. \end{aligned} \quad (58)$$



Rearranging the first and third summands of (58), applying the limit properties, and using the identity  $\int_{-\infty}^{\infty} f_{\check{S}_1}(s)ds = 1$  produce

$$\lim_{(\|\check{\mathbf{y}}_{K-1,n}^{(T)}\|\|\mathcal{H}_{-1}, \|\check{\mathbf{y}}_{K-1,n}^{(T)}\|\|\mathcal{H}_1\|) \rightarrow (0,\infty)} \check{P}_e \leq \frac{1}{2} \left[ \frac{1}{2} + \int_0^{\infty} \lim_{(\check{y}_{\max|\mathcal{H}_{-1}}, \check{y}_{\min|\mathcal{H}_1}) \rightarrow (0,\infty)} f_{\check{S}_{-1}}(s)ds \right], \quad (59)$$

where  $\check{S}_{-1}$  is defined in (49a). As  $\|\check{\mathbf{y}}_{K-1,n}^{(T)}\|\|\mathcal{H}_{-1} \rightarrow 0$ ,  $(\check{\mathbf{y}}_{K-1,n}^{(T)})_q|\mathcal{H}_{-1} \rightarrow 0$ ,  $\forall q$  and  $n$ . As a result, it follows via (49a) that  $\lim_{(\check{y}_{\max|\mathcal{H}_{-1}}, \check{y}_{\min|\mathcal{H}_1}) \rightarrow (0,\infty)} f_{\check{S}_{-1}}(s)$  becomes a Dirac delta function  $\delta(s)$ . Thus, substituting  $\delta(s)$  into the RHS (59) gives

$$\lim_{(\|\check{\mathbf{y}}_{K-1,n}^{(T)}\|\|\mathcal{H}_{-1}, \|\check{\mathbf{y}}_{K-1,n}^{(T)}\|\|\mathcal{H}_1\|) \rightarrow (0,\infty)} \check{P}_e \leq \frac{1}{4} + \frac{1}{2} \int_0^{\infty} \delta(s)ds. \quad (60)$$

Since the PDF of  $\delta(s)$  affirms  $\int_{-\infty}^{\infty} \delta(s)ds = 1$  and  $\delta(s)$  is an even function [3],  $\int_0^{\infty} \delta(s)ds = 1/2$ . Plugging this value into the RHS of (60) leads to

$$\lim_{(\|\check{\mathbf{y}}_{K-1,n}^{(T)}\|\|\mathcal{H}_{-1}, \|\check{\mathbf{y}}_{K-1,n}^{(T)}\|\|\mathcal{H}_1\|) \rightarrow (0,\infty)} \check{P}_e \leq 1/2. \quad (61)$$

Thus, (61) proves (28b). □

Therefore, both (28a) and (28b) are now proven. This ends the proof of Theorem 2. ■

## REFERENCES

- [1] J. G. Proakis, and M. Salehi, *Digital Communications*, 5th ed. New York, NY, USA: McGraw-Hill, 2008.
- [2] T. M. Getu and G. Kaddoum, "Fundamental limits of deep learning-based binary classifiers trained with hinge loss," 2023. [Online]. Available: <https://arxiv.org/pdf/2309.06774v1.pdf>
- [3] Wikipedia, "Dirac delta function," [Online]. [https://en.wikipedia.org/wiki/Dirac\\_delta\\_function](https://en.wikipedia.org/wiki/Dirac_delta_function) (accessed Jan. 2025).
- [4] Wolfram, "Wolfram MathWorld: Hyperbolic Tangent," [Online]. <https://mathworld.wolfram.com/HyperbolicTangent.html> (accessed May 2022).